




Run-Up of Impulse Wave Trains on Steep to Vertical Slopes

Journal Article

Author(s):

Kastinger, Maximilian ; Evers, Frederic M. ; Boes, Robert 

Publication date:

2020-10

Permanent link:

<https://doi.org/10.3929/ethz-b-000438635>

Rights / license:

In Copyright - Non-Commercial Use Permitted

Originally published in:

Journal of Hydraulic Engineering 146(10), [https://doi.org/10.1061/\(ASCE\)HY.1943-7900.0001803](https://doi.org/10.1061/(ASCE)HY.1943-7900.0001803)

Run-up of Impulse Wave Trains on Steep to Vertical Slopes

Maximilian B. A. Kastinger¹; Frederic M. Evers²; and Robert M. Boes³

Abstract: Impulse wave trains are generated by subaerial landslides, rockfalls, or avalanches, impacting a water body. Especially in engineered reservoirs, the run-up of waves with small relative heights is critical due to the small freeboard between the still water level and the dam crest. To prevent overtopping, an accurate prediction of the maximum run-up height is important for dam safety and hazard mitigation. The run-up behavior of impulse wave trains on a plane and impermeable barrier with slope angles between 18.4° and 90° was investigated in a two-dimensional wave channel. New breaker type criteria and a run-up prediction equation for the first five waves were developed. The main findings are: (1) The wave crest celerity decreases monotonically from the leading to the following waves. (2) For non-breaking and surging-breaking waves of the same wave crest amplitude, the leading wave does not induce the maximum run-up height. (3) The proposed run-up equation predicts the run-up height of non-breaking waves and surging breakers with a maximum underestimation of 25% and 40%, respectively. For plunging breakers, it may serve as an upper limit.

Author keywords: Impulse wave; Wave train; Run-up; Landslide; Physical modelling; Prediction method.

Introduction

Motivation

Very rapid gravity-driven mass movements including subaerial landslides, rockfalls, snow avalanches, or glacier breakoffs can cause large water waves in open oceans, bays, natural lakes, and reservoirs (Heller *et al.* 2009, Evers *et al.* 2019b). During these events, so-called impulse waves are generated, which propagate away from the impact location. While a first wave is generated due to the direct impact of the slide, it may be followed by several further waves due to the drawdown and run-up along the shore after the initial impact. Such series of multiple wave crests and troughs are referred to as impulse wave trains (Mohammed and Fritz 2012; McFall and Fritz 2016; Evers *et al.* 2019a). As the initial wave heights can be significantly larger than those of earthquake-induced tsunamis, such waves are also known as megatsunamis. At the shore, impulse wave trains can reach extreme run-up heights, causing damages to settlements and infrastructure. In the past, numerous impulse wave events have occurred worldwide. Roberts *et al.* (2014) compiled a global catalogue with 254 events generated by subaerial landslides. Extreme run-up heights have been observed in Lituya Bay in southeastern Alaska (1958, 524 m) (Miller 1960), Chehalis Lake in Canada (2007, 38 m) (Roberts *et al.* 2013), Taan Fjord in Alaska (2015, 193 m) (Higman *et al.* 2018), and Karrat Fjord in Greenland (2017, 90 m) laterally to the impact slope and 50 m on the opposite shore of the 6 km wide fjord (Fritz *et al.* 2018). Mountainous regions face a high risk of such events due to their numerous lakes and reservoirs, steep valley flanks, potentially large slide volumes, and high impact velocities (Heller and Hager 2010; Evers *et al.* 2018). Engineered reservoirs are of particular interest, as there is usually a freeboard of only a few meters between the still water level and the crest of the water-impounding structure, typically an embankment or concrete dam, with the risk of impulse wave overtopping already by small relative wave heights. In 1959, an impulse wave was generated in the reservoir of Pontesei Dam, Italy, by a landslide. Although the reservoir water level was 13 m below its maximum elevation, the dam crest was overtopped by “a few meters” (Walters 1971). In the same year, a landslide of ice and debris from the Marmolada Glacier, Italy, generated an impulse wave in the Fedaia reservoir, which overtopped the dam crest (Coppola *et al.* 2013). One of the most catastrophic impulse wave events occurred at the Vajont Dam, Italy, in 1963. A landslide-generated impulse wave ran up 235 m high on the opposite shore and overtopped the concrete dam. The resulting flood wave destroyed several villages downstream, causing about 2,000 fatalities (Panizzo *et al.* 2005). Since the impounding of Lake Roosevelt behind the Grand Coulee Dam, USA, in 1942, numerous landslides have caused impulse wave events, most recently in 2009. Although the dam itself has never been overtopped, run-up heights at the shore of up to 20 m have been observed (Lockridge 1990; Roberts *et al.* 2014). Several physical model studies, investigating potential hazard scenarios due to impulse waves, have been conducted for specific reservoirs (e.g. Volkart 1975; Davidson and McCartney 1975; Fuchs *et al.* 2011). To prevent overtopping, the prediction of the maximum

¹ Graduate Research Assistant, Laboratory of Hydraulics, Hydrology and Glaciology (VAW), ETH Zurich, CH-8093 Zürich, Switzerland, kastingm@student.ethz.ch, ORCID 0000-0002-0218-7425

² Senior Research Assistant, Laboratory of Hydraulics, Hydrology and Glaciology (VAW), ETH Zurich, CH-8093 Zürich, Switzerland, evers@vaw.baug.ethz.ch, ORCID 0000-0001-5181-8978 (corresponding author)

³ Professor and Director, Laboratory of Hydraulics, Hydrology and Glaciology (VAW), ETH Zurich, CH-8093 Zürich, Switzerland, boes@vaw.baug.ethz.ch, ORCID 0000-0002-0319-976X

impulse wave run-up height is necessary. While for small impulse wave events the operational freeboard may be sufficient to prevent overtopping, adequate preemptive reservoir drawdown needs to be initiated for larger waves (Kobel *et al.* 2017). In both cases the run-up height prediction needs to be as accurate as possible, to avoid overtopping and to limit the release of water without energy production and the involved economic losses, respectively. Fig. 1 shows the Grande Dixence Dam and the Lac des Dix in Switzerland. It illustrates a hypothetical scenario of the processes described above, where a reservoir featuring a small freeboard relative to its depth is surrounded by steep valley flanks, prone to potential mass wasting. The hazard of impulse waves in reservoirs is important in terms of dam safety and is therefore included in official regulations (Achterberg *et al.* 1998; Pougatsch *et al.* 2002).



Fig. 1. Photo of the Grande Dixence Dam and Lac des Dix in Switzerland (Photo: Roland Zumbuehl, CC BY-SA 4.0)

Impulse Wave Run-up

Impulse wave train propagation in a water body of still water depth h is characterized by an initial uprising of the water surface followed by several wave crests and troughs (Fig. 2). Each wave i within the wave train can be described by individual wave characteristics, including the wave crest amplitude a_{ci} , the wave trough amplitude a_{ti} , the wave height H_i , the wave crest celerity c_i , the wave period T_i , and the wavelength L_i . While the leading wave crest amplitude a_{c1} decays with propagation distance, subsequent wave amplitudes may temporarily increase due to dispersion (Løvholt *et al.* 2008). Hence, with increasing distance to the impact location the run-up of the subsequent waves may be more significant than the one of the leading wave (Ward 2001; Fritz and Borrero 2006). During the run-up process, the waves steepen due to shoaling and wave breaking can occur. For each wave i , the run-up height R_i is defined as the vertical distance between the still water level (SWL) and the highest point of the up-rush swell (Fig. 2). According to Müller (1995), the governing parameters influencing general wave run-up can be subdivided into wave, fluid and geometrical parameters. The latter include the bathymetry of the water body, the topography of the shoreline, the slope angle β and the roughness of the run-up surface.

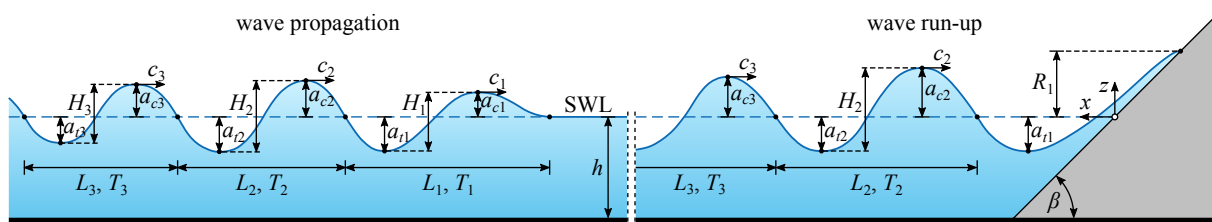


Fig. 2. Definition scheme for impulse wave train propagation and run-up

One of the first experimental studies on the run-up of non-breaking solitary waves, i.e. waves with a single wave crest ($a_c = H$), was conducted by Hall and Watts (1953). The run-up height was found to be governed by the still water depth h , wave crest amplitude a_c and shore slope angle β . Synolakis (1987) investigated non-breaking and breaking solitary wave run-up analytically and developed an approximate solution based on the non-linear wave theory. It involved laboratory experiments, which compared well with the analytical prediction. However, Synolakis (1987) focused on mildly sloped beaches and coastal structures ($\beta = 2.9^\circ$). The proposed “run-up law” tends to underestimate the run-up height of small relative wave crest amplitudes on steep slopes with $\beta > 25^\circ$ and it is not applicable to run-up at vertical walls with $\beta = 90^\circ$ (Evers and Boes 2019). In coastal engineering, many studies examined the run-up behavior of solitary waves (Pujara *et al.* 2015). Again, these studies are related to mildly sloped beaches, whereas reservoirs and especially dam structures feature steep to vertical slopes. Müller (1995) generated impulse wave trains and investigated the run-up and overtopping of an impulse wave train’s first wave for $\beta = 18.4^\circ$, 45° , and 90° . The run-up and back-wash process of single and double solitary waves of same wave height was investigated by Lo *et al.* (2013). It was found that the run-up height of the second wave varies with respect to the separation time to the first one. Fuchs and Hager (2015) conducted experiments on solitary wave run-up and overland flow, with a focus on scale and model effects. Evers and Boes (2019) compiled run-up data sets from several published sources and found the run-up behavior of solitary waves and the first wave of impulse wave trains to be similar for steep to vertical slopes. The relative run-up height R/h can be predicted by

$$\frac{R}{h} = 2\varepsilon e^{0.4\varepsilon} \left(\frac{90^\circ}{\beta} \right)^{0.2}, \quad (1)$$

with the relative wave crest amplitude $\varepsilon = a_c/h$. Eq. (1) covers a broad parameter range of $0.007 \leq \varepsilon \leq 0.69$ and $10^\circ \leq \beta \leq 90^\circ$. Note that Eq. (1) only applies to non-breaking wave run-up on steep to vertical slopes.

Run-up of breaking waves is characterized by different breaker types, including spilling, surging, or plunging, depending on the wave steepness and shore slope (Wiegel 1964). Galvin (1968) additionally describes the collapsing breaker type, a transition between the plunging and surging breaker. To determine whether or not periodic waves break at the slope, Iribarren and Nogales (1949) introduced the parameter

$$\xi = \frac{\tan \beta}{\sqrt{H/L}} \quad (2)$$

as a breaking criterion. It is also referred to as the Iribarren number or surf similarity parameter. Hunt (1959) investigated experimental run-up data from previous studies on periodic waves and found that the run-up height is proportional to ξ . Battjes (1974) showed that ξ is also useful to describe other processes of periodic waves on a slope, including wave reflection, wave setup, wave run-up, and wave run-down, and assigned numerical values to ξ to separate between the different breaker types. Since then, the surf similarity parameter has served as a basis for the quantification of wave run-up phenomena in several studies investigating the non-breaking and breaking run-up behavior of periodic waves and irregular wave spectra, including Schüttrumpf (2001) and Hammeken Arana (2017).

With respect to the run-up height prediction of impulse wave trains, equations derived from experiments with solitary waves have been commonly applied (e.g. Bregoli *et al.* 2017, McFall and Fritz 2017). The approximation of solitary-like waves is reasonable for rapid landslides of large mass impacting a water body of low still water depth, according to the findings of Heller and Hager (2011). However, it is stated that impulse waves generated by small mass movements result in irregular Stokes-like wave trains with wave crest amplitudes that are relatively small compared to the still water depth. For this wave type, the leading wave is not necessarily the one of maximum height and the decisive maximum run-up height might be caused by one of the subsequent waves. Due to the relatively small freeboard at reservoirs, even these small waves can cause dam overtopping. Therefore, this experimental research relates to the run-up of irregular impulse wave trains with multiple crests of small relative amplitude. It aims at investigating the wave run-up behavior, as well as proposing a run-up prediction equation for the leading and subsequent waves on steep slopes including vertical walls.

Physical Model

Experimental Setup

The two-dimensional (2D) run-up behavior of impulse wave trains on an artificial shore was investigated by physical modelling. Hydraulic experiments were conducted in an 11.0 m long, 0.5 m wide, and 1.0 m deep wave channel (Fig. 3). Its front side wall and two thirds of the channel bottom are made of glass allowing for optical observation. The remaining channel bottom and the other side walls are made of smooth steel plates. The wave generation mechanism consists of an adjustable chute, featuring a sliding plane of slope angle α and a release box with lateral guidance walls. For the wave generation, mesh-packed granular material was used as an alternative to free granular material slides mainly in view of experimental effort and handling. Evers and Hager (2015) showed that waves generated by mesh-packed slides are physically similar to these generated with free granular material. Two different granules were loosely filled into bags of sifting medium, each. One was made of 87% BaSO₄ and 13% polypropylene with a grain (subscript *g*) density $\rho_g = 2,429 \text{ kg/m}^3$, a bulk slide (subscript *s*) density $\rho_s = 1,338 \text{ kg/m}^3$, and a porosity $n = 45\%$ (Heller 2008). The other material was made of 100% polypropylene with $\rho_g = 955 \text{ kg/m}^3$, $\rho_s = 573 \text{ kg/m}^3$, and $n = 40\%$ (Heller 2008). The slide width $b = 0.5 \text{ m}$ and a slide thickness $s = 0.12 \text{ m}$ were constant. The sliding mass m_s was accelerated by gravity from various drop heights Δz after opening the release box. The slide front velocity V_s right before the impact was measured with two laser light barriers (LLB) OHDK 14 (Baumer Electric AG, Frauenfeld, Switzerland), which were aligned with the sliding plane. The sample frequency of 1,000 Hz resulted in a measurement accuracy of $\pm 1.5\%$ for the maximum measured slide impact velocity of 3.03 m/s over a measuring section of 0.2 m. Prior to each test run, the still water depth h was controlled with a point gauge of measurement accuracy $\pm 0.5 \text{ mm}$ to ensure reproducible experiments. The water surface displacement η was measured with ultrasonic distance sensors (UDS) UNAM 30 (Baumer Electric AG, Frauenfeld, Switzerland), located along the channel axis. Their sample frequency was 60 Hz with a measurement accuracy of $\pm 0.8 \text{ mm}$. The UDS recordings were smoothed with a Savitzky-Golay filter (Savitzky and Golay 1964). A splash protection was installed downstream of the wave generation zone to avoid disturbance of the UDS measurements by water splashes due to the slide impact. The unconfined wave train propagation, i.e. without the installed barrier, was recorded by all seven UDS. A wave absorber was placed at the end of the channel to reduce the time required to calm the water surface after each unconfined experiment. For the run-up experiments a barrier with an adjustable slope angle $\beta = 90^\circ$ (1:0), 45° (1:1), 26.6° (1:2), and 18.4° (1:3) was installed. A measuring tape with 1 mm scaling was attached to the barrier plate to read off the onshore propagation distance of the run-up front. The latter was done based on video recordings with a HERO4 Black camera (GoPro, San Mateo, California), which was installed inside the channel and operated at 60 fps. Selected run-up experiments were recorded with a single-lens reflex camera EOS 5D Mark IV (Canon, Tokyo) and a 16–35 mm lens through the glass side window.

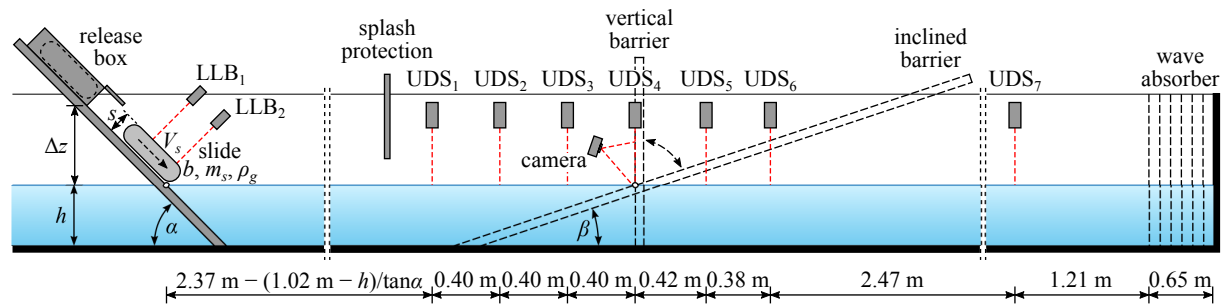


Fig. 3. Experimental setup for unconfined impulse wave train propagation and for run-up experiments with a vertical or inclined barrier (dashed contours)

Experimental Procedure

To generate impulse wave trains with a broad range of characteristics, 35 different configurations of slide parameters and still water depths were applied. Each test was conducted twice, to detect considerable random errors and to check for reproducibility. The focus was on relative wave crest amplitudes $\varepsilon_i < 0.10$, critical for impulse waves in reservoirs with respect to the prevention of dam overtopping for small freeboard values. Heller and Hager (2010) introduced the impulse product parameter $P = FS^{1/2}M^{1/4}\{\cos[(6/7)\alpha]\}^{1/2}$, with slide Froude

number $F = V_s/(gh)^{1/2}$, relative slide thickness $S = s/h$, relative slide mass $M = m_s/\rho_w b h^2$, and slide impact angle α . This parameter is used for the prediction of individual wave features and the maximum wave crest amplitude and height significantly increase with increasing P . It can be noted that F , and consequently V_s and h , have the strongest effect on P . Therefore, a minimum still water depth $h_{\min} = 0.3$ m was chosen and the slide impact velocity V_s was kept low ($V_{s,\max} = 3.03$ m/s), in order to limit the values of F ($F_{\max} = 1.77$) and consequently P . Test ranges of the absolute and relative governing parameters are specified in Table 1. All experiments were conducted with fresh water of approximately 20°C and a constant density $\rho_w = 1,000$ kg/m³. The gravity acceleration was accounted for with $g = 9.81$ m/s².

Table 1. Experimental parameter ranges for impulse wave generation

Parameter	Unit	Test range	Dimensionless parameter	Test range
h	(m)	0.3–0.7	—	—
α	(°)	30–90	α	30–90
V_s	(m/s)	0.88–3.03	F	0.41–1.77
m_s	(kg)	5–10	M	0.020–0.222
ρ_g	(kg/m ³)	955; 2,429	ρ_g/ρ_w	0.96–2.43
ρ_s	(kg/m ³)	573; 1,338	ρ_s/ρ_w	0.57–1.34
n	(%)	40; 45	—	—
—	—	—	P	0.052–0.513

The wave train profiles were recorded by UDS₁ to UDS₆, located in the central part of the wave channel, as shown in Fig. 3. Wave characteristics were only measured along the length and depth axes of the channel, while constant conditions were considered along the channel width. Fig. 4 shows an exemplary recording of the relative water surface displacement η/h with respect to the still water level (SWL, $\eta = 0$). The beginning of the leading wave crest (uplifting) was defined with $\eta > 0.5$ mm. The subsequent zero-crossing nodes and the wave crest and trough amplitudes were determined by automated peak detection. With the wave crest detected by two subsequent sensors, the spatially averaged wave crest celerity c between both locations was determined. At each UDS, c was then approximated as the mean of the corresponding up- and downstream values of the considered location. As the propagation distance within the wave channel was limited, subsequent wave features were eventually affected by the reflection of the leading wave (grey areas in Fig. 4). The corresponding point in time of disturbance was determined by adding the travel time of the leading wave to the measured time of the initial uplifting. This travel time involves the celerity of the leading wave c_1 as well as a residence time t_r at the wave absorber. The former was determined between UDS₆ and UDS₇ and was considered constant from then on. The residence time t_r for the reflection of solitary waves at a vertical wall was estimated according to Chen *et al.* (2015) with

$$t_r = \frac{2}{\sqrt{3}} \left(\ln \left(\frac{\sqrt{3}+1}{\sqrt{3}-1} \right) \varepsilon^{-1/2} + \frac{1}{8} \ln \left(\frac{\sqrt{3}+1}{\sqrt{3}-1} \right) \varepsilon^{1/2} \right) \sqrt{\frac{h}{g}}, \quad (3)$$

for $0.147 \leq \varepsilon \leq 0.556$. For the unconfined experiments ε_1 at UDS₇ was considered. However, for the values of this study with $\varepsilon_1 < 0.1$, Eq. (3) appeared to result in unrealistic long residence times. Consequently, as a lower limit ①, the residence time was neglected ($t_r = 0$) and the result of Eq. (3) was used as an upper limit ②. In the example of Fig. 4, the first four waves were considered unconfined, whereas the fifth one shows a deviating trend, indicating a disturbance due to wave reflection of the leading wave. The number of unconfined waves not affected by reflection was determined for all tests with this approach.

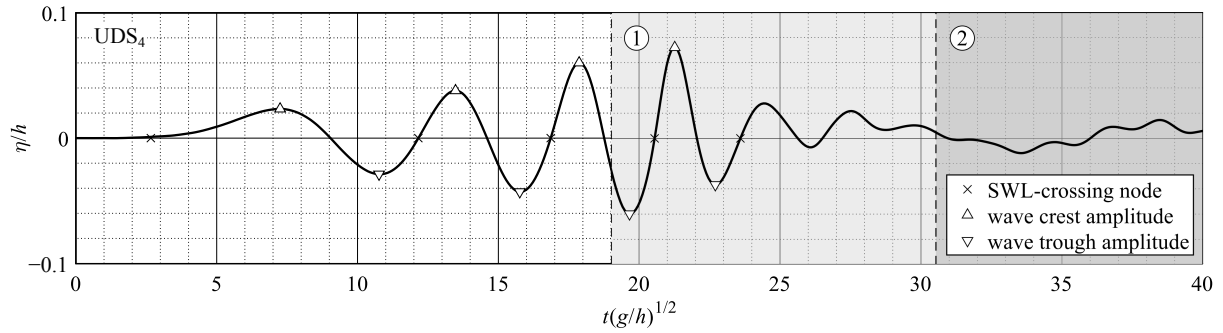


Fig. 4. Exemplary impulse wave train profile at UDS₄ with detected (×) SWL-crossing nodes, (Δ) wave crest amplitudes and (▽) wave trough amplitudes; the grey areas are affected by wave reflection of the first wave for ① $t_r = 0$ and ② t_r determined by Eq. (3)

For the same slide parameters as the unconfined experiments, 35 run-up experiments with a vertical barrier ($\beta = 90^\circ$) were conducted. In addition, run-up experiments with three inclined slope angles $\beta = 45^\circ$ (1:1), 26.6° (1:2), and 18.4° (1:3), were conducted each for 22 of the previous slide parameter configurations. The configurations were chosen, so that the same wave parameter ranges were covered. Depending on the still water depth h , the barrier was installed with the intersection point of the still water level and the barrier plate (shore point) at the same locations as UDS₃, UDS₄, UDS₅, or UDS₆ (Fig. 3). To check the reproducibility of the generated impulse wave trains, the leading relative wave crest amplitude ε_1 at UDS₁ and the slide impact velocity V_s were compared to the ones of the corresponding unconfined experiments. If ε_1 at UDS₁ was not affected by wave reflection, a deviation of $\pm 10\%$ was considered acceptable. Otherwise, V_s served as the measure of reproducibility, also tolerating deviations within a range of $\pm 10\%$. The disturbance due to wave reflection was determined similar to the unconfined experiments described above, considering the UDS closest to the run-up slope. To calculate the residence time t_r by Eq. (3) at the inclined barrier and chute, both were treated as vertical walls located at the shore points. For the run-up experiments, influence of wave reflection was considered present after the initial uplifting had been reflected twice, first at the barrier and then at the chute.

Based on the recorded videos of the in-channel camera, the on-shore propagation distances of the individual run-up fronts along the barrier plate were determined. To exclude sidewall effects, only the central part of 0.3 m width was considered during video analysis. Fig. 5(a) shows a run-up recording of a non-breaking wave. The water tongue is almost straight, with a small difference between the mean run-up height R_m and the minimum R_{\min} and maximum R_{\max} run-up heights. In contrast, the up-rush swell of breaking waves is more irregular, as shown in Fig. 5(b). Deviations of R_{\max} or R_{\min} with respect to R_m of up to $\pm 25\%$ were observed. Splashes due to wave breaking were neglected during video analysis. For the subsequent data analysis R_m of each run-up experiment was considered. With the side-channel camera recordings of selected experiments, the behavior during run-up and back-wash could be investigated qualitatively. They served as a basis to differentiate between the various breaker types.

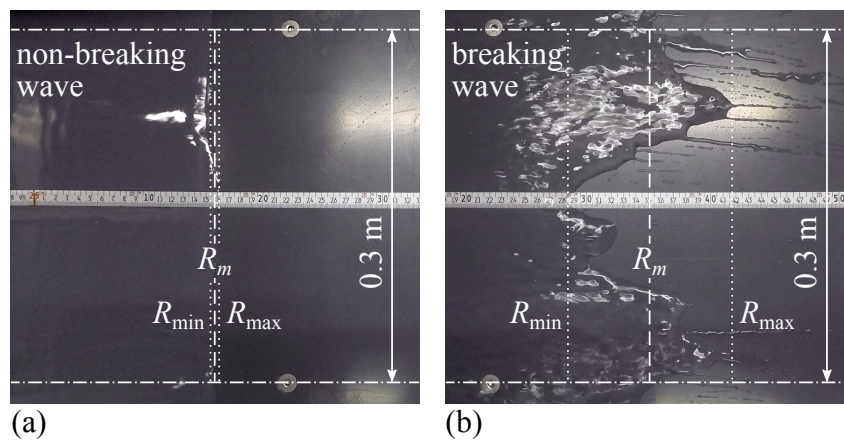


Fig. 5. Video recordings of (a) non-breaking and (b) breaking wave run-up with minimum R_{\min} , maximum R_{\max} and mean R_m run-up heights

Out of the two unconfined experiments, the one with the better agreement of ε_1 at UDS_1 or V_s of the confined experiment was considered to analyze the relation between the undisturbed wave train and the wave run-up for identical initial slide parameters. Consequently, four run-up experiments with the same initial slide parameters, but different slope angles β , do not all necessarily relate to the same unconfined experiment. By applying this selection procedure, 49 of the 70 unconfined tests were eventually used for the analysis, considering at least the first three waves as undisturbed, i.e. not affected by reflection from the wave absorber (Fig. 3). The fourth and fifth waves were also included in 35 and 5 of the experiments, respectively. Regarding the run-up experiments, a total of 101 tests were analyzed. Again, the first three waves were always considered undisturbed, i.e. not affected by reflection from the chute (Fig. 3), while for 81 of the experiments also the fourth waves and in 12 cases even the fifth waves were included. The complete data set including the experimental parameters is provided by Kastinger *et al.* (2020).

Scale Effects

According to Le Méhauté (1976), scale effects for non-breaking wave propagation are negligible for still water depths $h > 0.02$ m and wave periods $T > 0.35$ s. As the minimum still water depth was $h_{\min} = 0.3$ m and the minimum wave period was $T_{\min} = 0.62$ s, scale effects during the wave propagation process were therefore considered insignificant. For breaking waves, i.e. plunging breakers, Stagonas *et al.* (2011) state that scale effects due to surface tension forces are negligible for wavelengths $L > 4$ m and wave heights $H > 0.11$ m. For the present study, all plunging breaking waves are below these two limits with a minimum wavelength $L_{\min} = 0.63$ m and a minimum wave height $H_{\min} = 0.023$ m. Scale effects might therefore be significant, resulting in reduced energy dissipation during the breaking process. Consequently, more energy remains for the wave run-up, presumably leading to larger run-up heights in the model compared to prototype scale. As wave breaking also includes air entrainment, further scale effects have to be expected due to the neglected scaling of the air-water mixture compressibility.

During wave run-up, the thickness of the water tongue h_R and the flow velocity of the up-rush swell c_R are crucial for the investigation of scale effects. As these two parameters were not measured for the present experiments, they are estimated according to Neelamani (2005), with

$$h_R = 0.32H \left(\xi e^{-\frac{z}{H}} \right)^{0.93} \quad (4)$$

$$c_R = 3.11\pi \frac{H}{T} \left(\xi^2 e^{-\frac{z}{H}} \right)^{0.52}, \quad (5)$$

including z as the vertical distance from the still water level to the considered point of the water tongue (Fig. 2). As both parameters become very low at the highest point of run-up, their values were estimated at 75% of the measured run-up heights ($z = 0.75R$). Schüttrumpf (2001) proposed lower limits for the run-up Reynolds number $R_R = c_R h_R / \nu > 10^3$, with $\nu = 10^{-6}$ m²/s as the kinematic water viscosity at 20°C, and the run-up Weber number $W_R = \rho_w c_R^2 h_R / \sigma > 10$, with $\sigma = 0.074$ kg/s² as the water surface tension at 20°C. Above these thresholds, scale effects due to friction and surface tension forces, respectively, are negligible. About 2% of the investigated waves lay below the first criterion, with a minimum run-up Reynolds number $R_{R,\min} = 2 \cdot 10^2$. With respect to the second criterion, for 8% of the run-up experiments W_R was below 10, with a minimum run-up Weber number $W_{R,\min} = 0.5$. However, as Müller (1995) states, the low values of R_R and W_R are limited to only short on-shore propagation distances of the run-up front. Especially for steep to vertical slopes, the influence might be considered insignificant compared to the overall run-up process.

Results

Impulse Wave Train Characteristics

The non-dimensional parameter ranges of the 49 generated unconfined impulse wave trains are specified in Table 2, subdivided for the first five waves i , including the relative wave crest amplitude $\varepsilon_i = a_{ci}/h$, the relative wave height H_i/h , the wave non-linearity a_{ci}/H_i , the relative wave period $T_i(g/h)^{1/2}$, the relative wave crest celerity $c_i/(gh)^{1/2}$, the relative wavelength L_i/h (with $L_i = c_i T_i$), and the wave steepness H_i/L_i . Their values refer to the corresponding UDS location, at which the barrier was installed for the run-up experiments. Note, that due to wave reflection $n_4 = 35$ of the unconfined experiments ($n = 49$) were included for the analysis of the fourth waves, while only $n_5 = 5$ of the fifth waves were considered.

Table 2. Non-dimensional test ranges of the generated unconfined impulse wave trains for the first five waves i

Parameter (—)	Test range of wave i within the wave train				
	1	2	3	4	5
$\varepsilon_i = a_{ci}/h$	0.011–0.080	0.020–0.076	0.024–0.110	0.028–0.117	0.053–0.086
H_i/h	0.028–0.168	0.044–0.160	0.044–0.214	0.045–0.186	0.078–0.131
a_{ci}/H_i	0.34–0.51	0.45–0.60	0.47–0.65	0.52–0.73	0.64–0.69
$T_i(g/h)^{1/2}$	7.2–12.7	3.7–5.9	2.7–4.9	2.4–4.3	3.2–3.9
$c_i/(gh)^{1/2}$	0.90–1.06	0.60–0.87	0.45–0.76	0.39–0.67	0.54–0.63
L_i/h	6.7–13.4	2.2–5.0	1.2–3.7	0.9–2.9	1.7–2.4
H_i/L_i	0.004–0.014	0.015–0.046	0.026–0.065	0.035–0.085	0.045–0.056

Fig. 6 shows the square of the relative wave crest celerity $c_i^2/(gh)$ versus the relative wavelength L_i/h for the waves of the present study and the experiments of Müller (1995), for comparison. It includes the celerity law of linear waves, the ranges for deep-water waves ($L/h < 2$), intermediate-water waves ($2 \leq L/h \leq 20$), and shallow-water waves ($L/h > 20$), as well as the solitary wave celerity $c_{sol} = [g(h + a_c)]^{1/2}$, for $a_c = 0.78h$ at wave breaking (McCowan 1894). It can be noted that the first waves clearly separate from the subsequent ones, with wave crest celerities close to the shallow-water wave celerity $c = (gh)^{1/2}$. The subsequent waves follow the celerity law of linear waves, with decreasing wave crest celerity and wavelength from the front to the back of the wave train and a transition from intermediate- to deep-water waves.

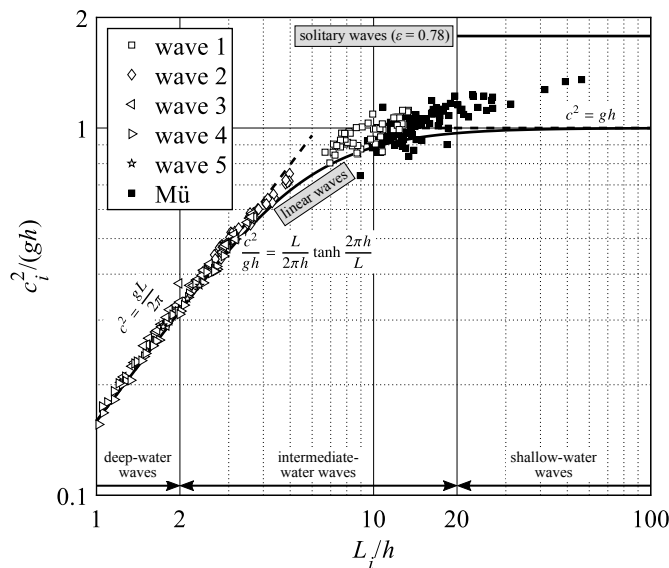


Fig. 6. Square of relative wave crest celerity $c_i^2/(gh)$ versus relative wavelength L_i/h for the waves of the present study and the experiments of Müller (Mü) (1995), including the celerity laws of linear and solitary waves (adapted from Fritz 2002)

Boxplots of the wave crest celerities over the solitary wave celerity $C_i = c_i / [g(h + a_c)]^{1/2}$ for the first four waves are presented in Fig. 7, including the number of experiments n_i and their median values \tilde{C}_i . The fifth waves are excluded, as too little data was available for a boxplot representation ($n_5 = 5$). For the leading waves, c_1 is about c_{Sol} with a median of $\tilde{C}_1 = 0.97$. The subsequent waves show a decreasing trend of C_i with $\tilde{C}_2 = 0.73$, $\tilde{C}_3 = 0.60$, and $\tilde{C}_4 = 0.50$ for the second, third, and fourth waves within the wave train, respectively. The median value of the fifth waves is $\tilde{C}_5 = 0.57$. Although \tilde{C}_5 is slightly larger than \tilde{C}_4 , it was verified, that the decreasing trend of the wave crest celerity is monotonic for each experiment, i.e. if the fifth wave had been measured in all experiments, $\tilde{C}_5 < \tilde{C}_4$ would be expected.

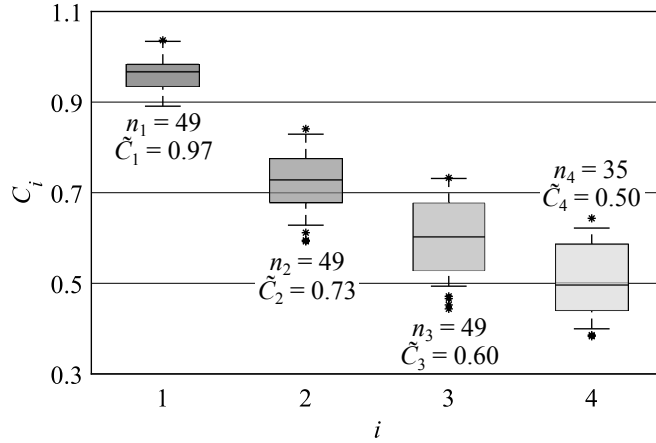


Fig. 7. Boxplots with whiskers at 2.5th and 97.5th percentile of the wave crest celerities over the solitary wave celerity $C_i = c_i / [g(h + a_c)]^{1/2}$ for the first four waves i within the wave train, including the number of experiments n_i and median value \tilde{C}_i

The relative wave heights H_i/h versus the inverse of the relative wavelengths h/L_i for the waves of the present study and the experiments of Müller (1995), for comparison, are shown in Fig. 8. Adapted from Komar (1998), it includes the areas of application of the various water wave theories, namely linear wave, Stokes wave, cnoidal wave, and solitary wave theory. Similar to Fig. 6, the leading waves may be clearly distinguished from the subsequent ones for this study's experiments. While the first and second waves lie in the area of linear intermediate-water waves, the third waves can be classified as linear intermediate- to deep-water waves. For the fourth waves, both, linear and Stokes waves can be noted. They might therefore be classified as Stokes-like waves (Heller and Hager 2011). The fifth waves again lie within the area of linear wave theory, however only $n_5 = 5$ data points were available and no clear statement can be made.

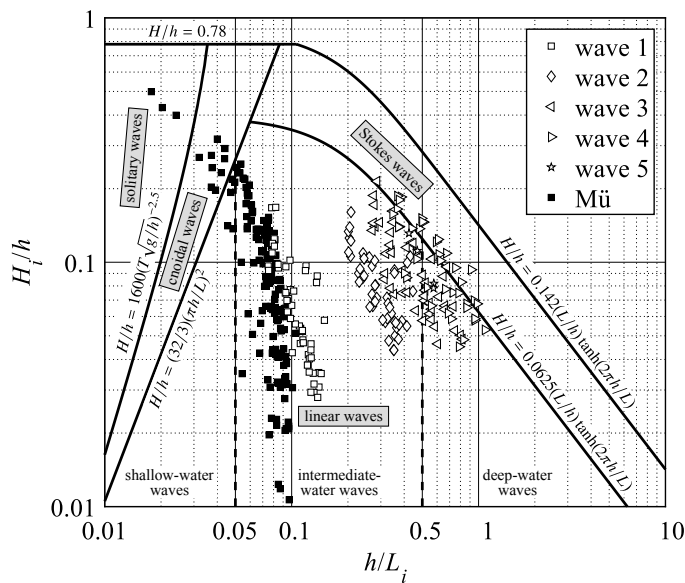


Fig. 8. Relative wave height H_i/h versus inverse of the relative wavelength h/L_i for the waves of the present study and the experiments of Müller (Mü) (1995), including the areas of application of the various water wave theories (adapted from Komar 1998)

Run-up Behavior

Based on the side-channel camera recordings, different run-up behavior for the various slope angles β was observed. For all run-up experiments, the leading wave ran up along the barrier without breaking, classified as non-breaking (NO). The following waves are additionally influenced by the back-wash of the previous ones and were breaking in some cases. Breaking waves were subdivided into surging breakers (SU), characterized by a steepening of the wave front face without overturning and no air entrainment, and plunging breakers (PL), featuring curling of the wave crest and significant air entrainment. As a transitional breaker type between surging and plunging breakers, the collapsing breaker was not distinguished.

Figs. 9, 10, 11, and 12 show the typically observed run-up behavior of the first four waves from selected experiments for $\beta = 90^\circ$ (1:0), $\beta = 45^\circ$ (1:1), $\beta = 26.6^\circ$ (1:2), and $\beta = 18.4^\circ$ (1:3), respectively. Non-breaking (NO) waves are captured at the maximum run-up height, while surging (SU) and plunging (PL) breakers are shown at the point of wave breaking. For the vertical barrier ($\beta = 90^\circ$), all waves were non-breaking. It can be noted that the intersection point of the displaced water surface with the initial still water level (SWL) approaches the barrier for the subsequent waves, while the run-up shape changes from convex [Figs. 9(a)–(c)] to concave [Fig. 9(d)]. For a barrier inclination of 1:1 ($\beta = 45^\circ$), the first three waves were always non-breaking [Figs. 10(a)–(c)], while also surging breakers occurred for the fourth wave [Fig. 10(d)]. When the barrier was inclined 1:2 ($\beta = 26.6^\circ$), only the first two waves were non-breaking [Figs. 11(a)–(b)]. The third wave was typically a surging breaker [Fig. 11(c)] and the fourth wave a plunging breaker [Fig. 11(d)]. For the mildest inclination of 1:3 ($\beta = 18.4^\circ$), this trend shifts forward, with the second wave typically being a surging breaker [Fig. 12(b)], followed by plunging breakers [Figs. 12(c)–(d)].

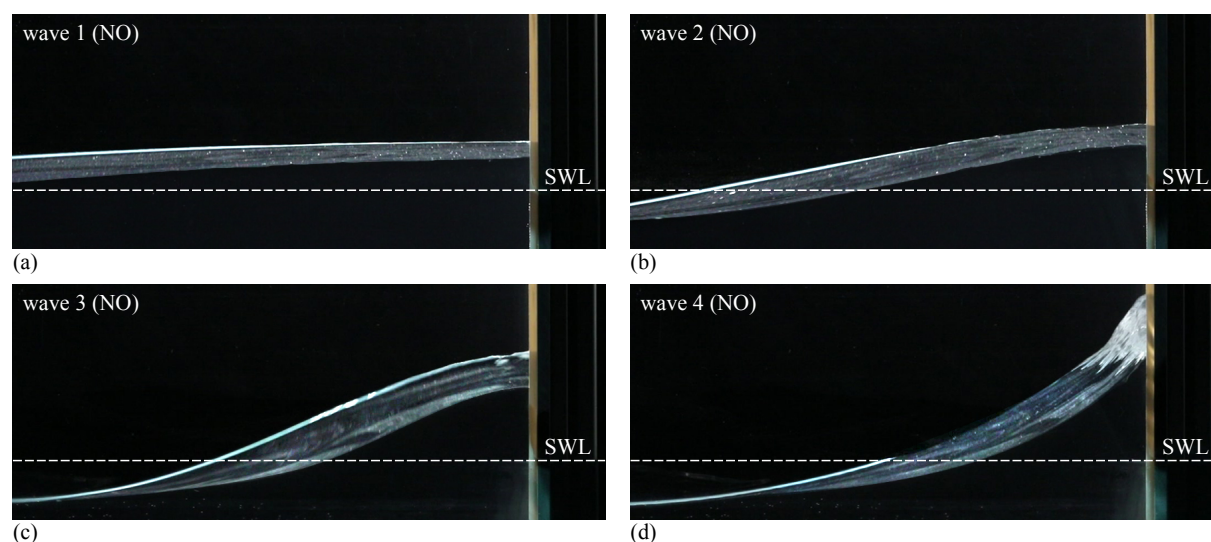


Fig. 9. Typical run-up behavior for a vertical barrier ($\beta = 90^\circ$) of (a) wave 1 (NO), (b) wave 2 (NO), (c) wave 3 (NO), and (d) wave 4 (NO), with (---) still water level (SWL)

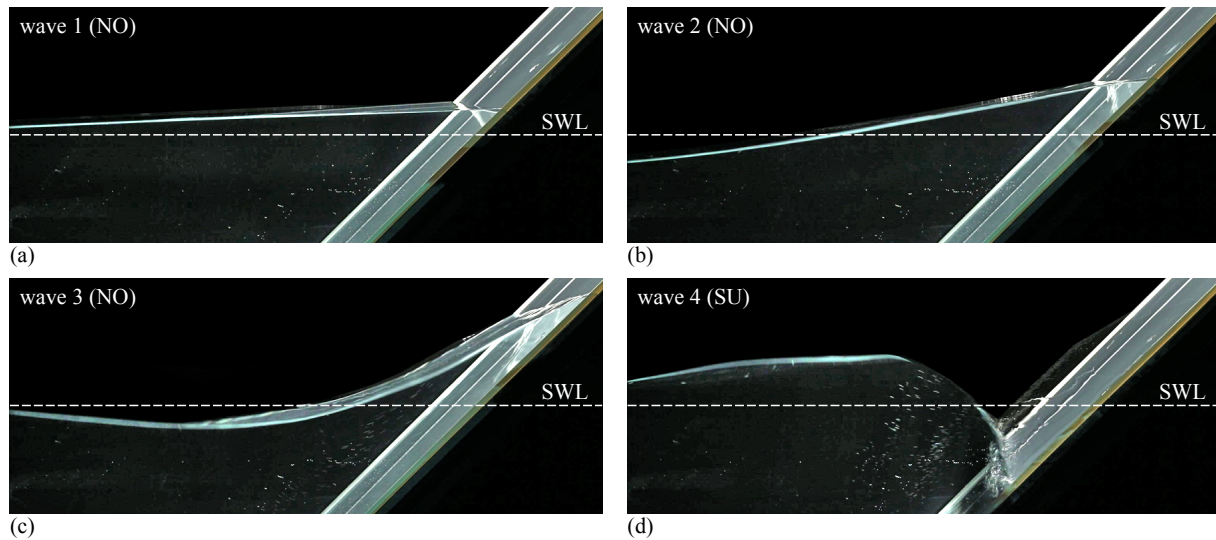


Fig. 10. Typical run-up behavior for a barrier inclination 1:1 ($\beta = 45^\circ$) of (a) wave 1 (NO), (b) wave 2 (NO), (c) wave 3 (NO), and (d) wave 4 (SU), with (---) still water level (SWL)

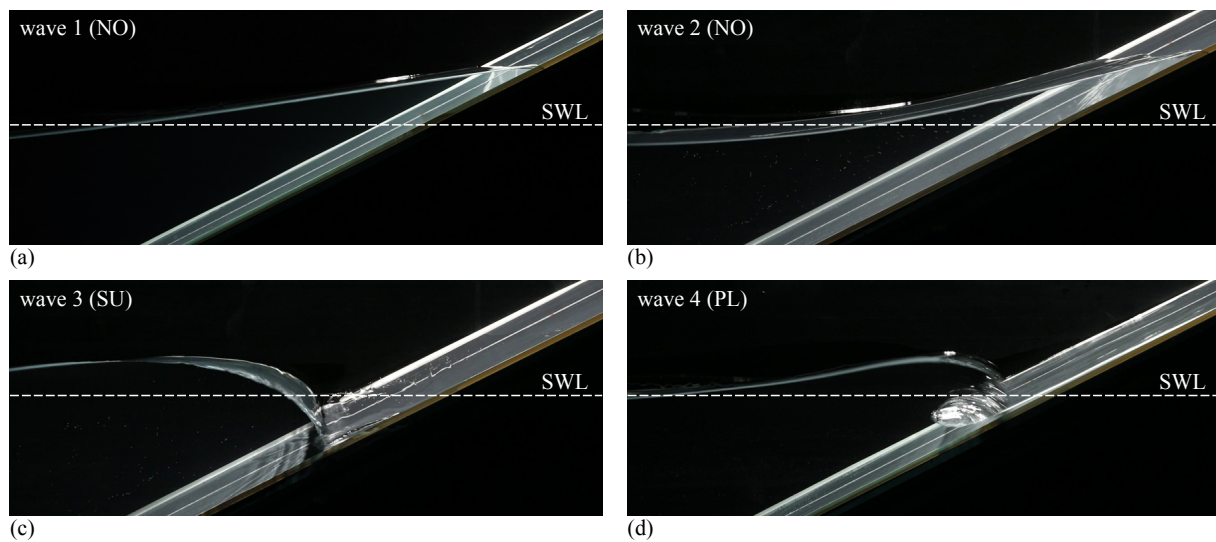


Fig. 11. Typical run-up behavior for a barrier inclination 1:2 ($\beta = 26.6^\circ$) of (a) wave 1 (NO), (b) wave 2 (NO), (c) wave 3 (SU), and (d) wave 4 (PL), with (---) still water level (SWL)

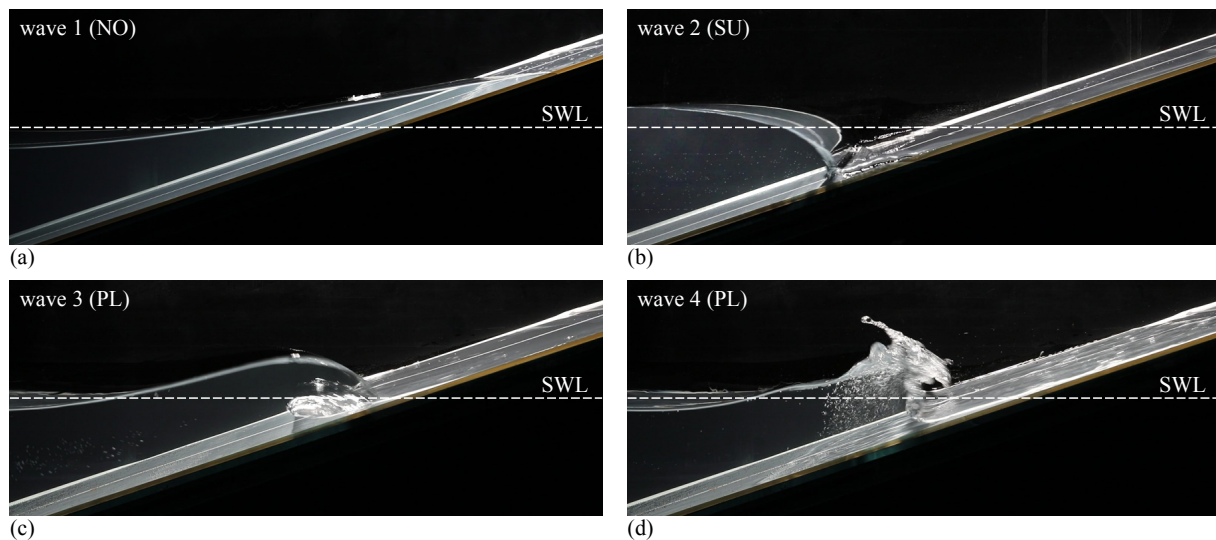


Fig. 12. Typical run-up behavior for a barrier inclination 1:3 ($\beta = 18.4^\circ$) of (a) wave 1 (NO), (b) wave 2 (SU), (c) wave 3 (PL), and (d) wave 4 (PL), with (---) still water level (SWL)

The histograms in Fig. 13 show the variation of the breaker types with respect to the waves i within the wave trains and the slope angle β . There was no wave breaking at the vertical barrier ($\beta = 90^\circ$). For $\beta = 45^\circ$, about 50% of the fourth and fifth waves were surging breakers. Wave breaking occurred from the third waves onwards for $\beta = 26.6^\circ$ with mainly surging breakers, followed by plunging breakers for the fourth and fifth waves. For $\beta = 18.4^\circ$, wave breaking already started with the run-up of the second waves, being mainly surging breakers. From the third wave onwards, only plunging breakers occurred.

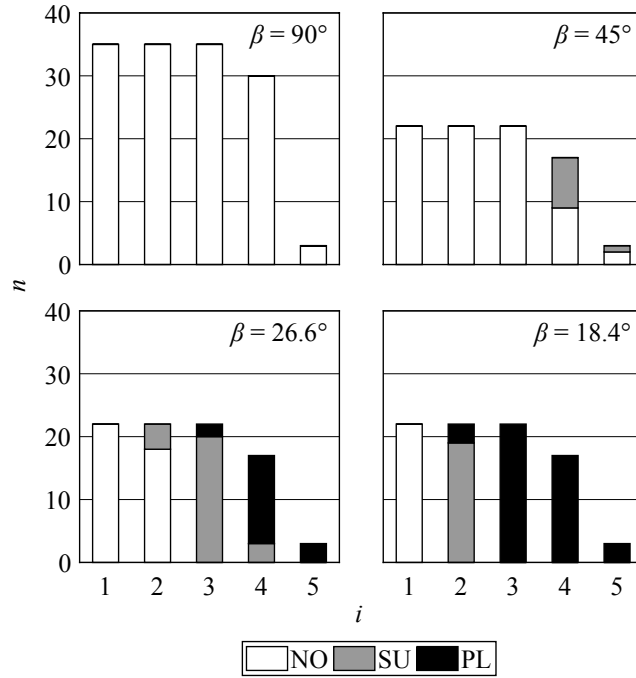


Fig. 13. Histograms of the number n of observed breaker types non-breaking (NO), surging breaker (SU), and plunging breaker (PL) for barrier slope angles $\beta = 90^\circ$, 45° , 26.6° , and 18.4° with respect to wave i within the wave train

Based on the surf similarity parameter ξ_i by Iribarren and Nogales (1949) [Eq. (2)], the wave non-linearity a_{ci}/H_i , and the relative wavelength L_i/h , breaker type prediction criteria are proposed as

$$\xi_i > 7(a_{ci} / H_i)e^{-0.04L_i/h} \quad \text{for non-breaking (NO) waves,} \quad (6)$$

$$4.5(a_{ci} / H_i)e^{-0.04L_i/h} \leq \xi_i \leq 7(a_{ci} / H_i)e^{-0.04L_i/h} \quad \text{for surging breakers (SU), and} \quad (7)$$

$$\xi_i < 4.5(a_{ci} / H_i)e^{-0.04L_i/h} \quad \text{for plunging breakers (PL).} \quad (8)$$

In Fig. 14, the term $\xi_i \exp(0.04 L_i/h)$, is plotted versus the non-linearity a_{ci}/H_i for the waves of the present study and the experiments of Müller (1995). Almost sharp boundaries between non-breaking waves, surging breakers and plunging breakers can be drawn with Eqs. (6) to (8).

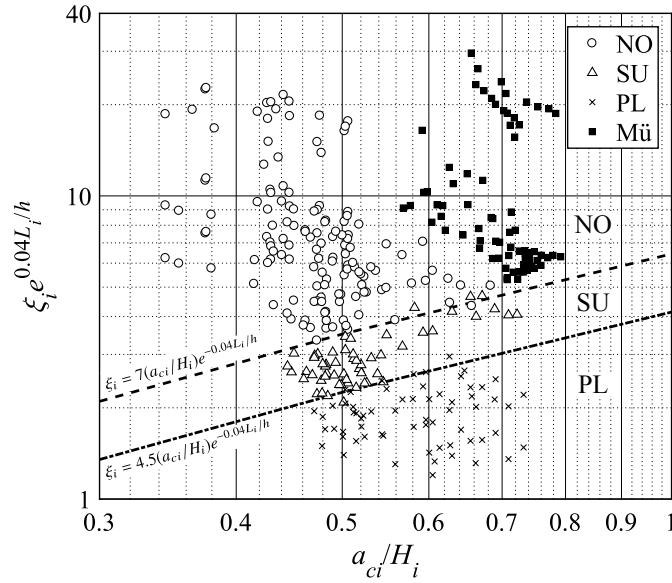


Fig. 14. Term $\xi_i \exp(0.04L_i/h)$ versus non-linearity a_{ci}/H_i for non-breaking (NO) waves, surging breakers (SU), and plunging breakers (PL) of the present study and the experiments of Müller (Mü) (1995), with (---) Eq. (6) (= instead of >) and (---) Eq. (8) (= instead of <)

Run-up Heights

The non-dimensional parameter ranges of the 101 run-up experiments are specified in Table 3, subdivided for the first five waves i within the wave train. As shown in Fig. 5, it includes the relative mean run-up height $R_{i,m}/h$ and the relative deviation of the maximum run-up height $(R_{i,max} - R_{i,m})/R_{i,m}$. In addition, the test ranges of the surf similarity parameter ξ_i for experiments with an inclined barrier ($\beta < 90^\circ$) are given. Note that due to wave reflection the fourth waves were considered for $n_4 = 81$ of the run-up experiments, while it was only $n_5 = 12$ for the fifth waves.

Table 3. Non-dimensional test ranges of the run-up parameters for the first five waves i within the wave train

Parameter (—)	Test range of wave i within the wave train				
	1	2	3	4	5
$R_{i,m}/h$	0.016–0.248	0.040–0.403	0.038–0.618	0.042–0.470	0.137–0.303
$(R_{i,max} - R_{i,m})/R_{i,m}$	0	0–0.25	0–0.39	0–0.25	0–0.25
ξ_i (for $\beta < 90^\circ$)	2.84–16.39	1.83–8.06	1.32–6.15	1.15–5.26	1.42–4.72

Fig. 15 shows the distribution of the mean run-up height over the wave crest amplitude $R_{i,m}/a_{ci}$ of each wave i within the wave train for the four investigated barrier slope angles β . Also, the corresponding breaker types are indicated. The fifth waves are excluded due to $n_5 = 12$. For non-breaking (NO) waves and surging breakers (SU), there seems a trend that $R_{i,m}/a_{ci}$ increases with decreasing β and increasing wave number i . However, this does not apply to plunging breakers (PL), which generally result in lower values and a large scatter of $R_{i,m}/a_{ci}$. The latter results from the turbulent wave breaking process and the reduced measuring accuracy from the in-channel camera recordings. For the distinct upward outlier of wave 2 for $\beta = 26.6^\circ$, no reasonable explanation was found.

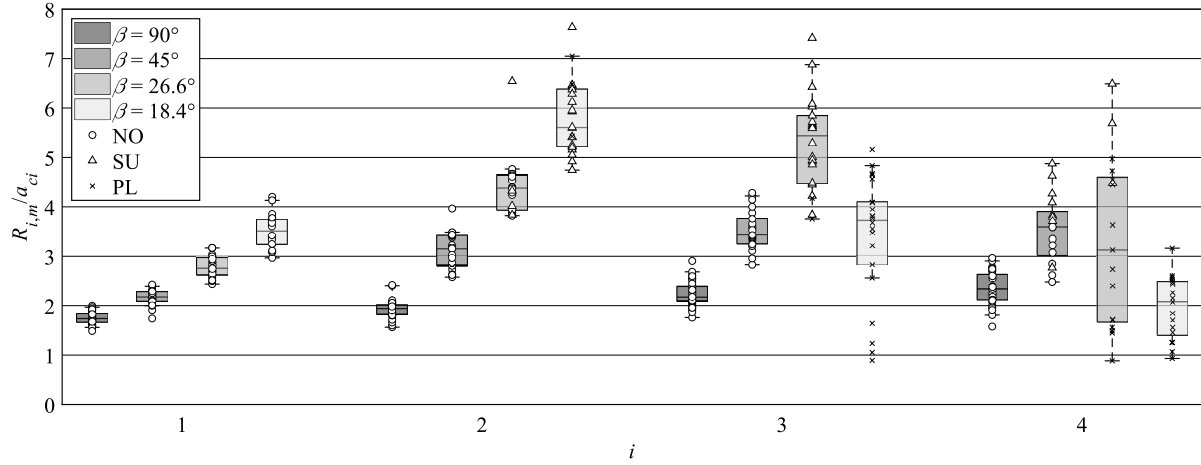


Fig. 15. Boxplots with whiskers at 2.5th and 97.5th percentile of the mean run-up height over the wave crest amplitude $R_{i,m}/a_{ci}$ for the first four waves i within the wave train and slope angles $\beta = 90^\circ, 45^\circ, 26.6^\circ$, and 18.4° ; the single measurements with corresponding breaker types (NO, SU, and PL) are also included

In comparison with Eq. (1) by Evers and Boes (2019), an increasing effect of the leading wave's non-linearity a_{c1}/H_1 on the relative run-up height R_1/h was found for decreasing β , especially for small values of a_{c1}/H_1 . Furthermore, the relative run-up height of the subsequent waves R_i/h showed a negative correlation with the relative wave crest celerity $c_i/(gh)^{1/2}$. Extending Eq. (1) with these findings, the following equation is introduced to approximate the relative run-up heights of all non-breaking waves ($R^2 = 0.92$):

$$\frac{R_i}{h} = 2\varepsilon_i e^{0.4\varepsilon_i} \left(\frac{c_i}{\sqrt{gh}} \right)^{-0.25} \left(\frac{90^\circ}{\beta} \right)^{0.2} \left(\frac{a_{c1}}{H_1} \right)^{-0.9} \left(\frac{c_i}{\sqrt{gh}} \right)^{-1.25} \quad (9)$$

Fig. 16 shows the measured over predicted run-up height $R_{i,meas}/R_{i,pred}$, for Eq. (9) being applied to all waves of the present study, versus the relative wave crest amplitude ε_i . The run-up heights of non-breaking (NO) waves are represented well within a $\pm 25\%$ scatter range, with few data points being overestimated. For surging breakers (SU), the run-up prediction quality decreases ($R^2 = 0.78$) and the relative run-up heights tend to be underestimated up to +40%. Besides one underestimated outlier with $\varepsilon_i = 0.062$, the run-up heights of plunging breakers (PL) are generally overestimated by Eq. (9). For plunging breakers $R^2 = 0$, i.e. no statistical correlation between the measured and predicted run-up heights can be determined.

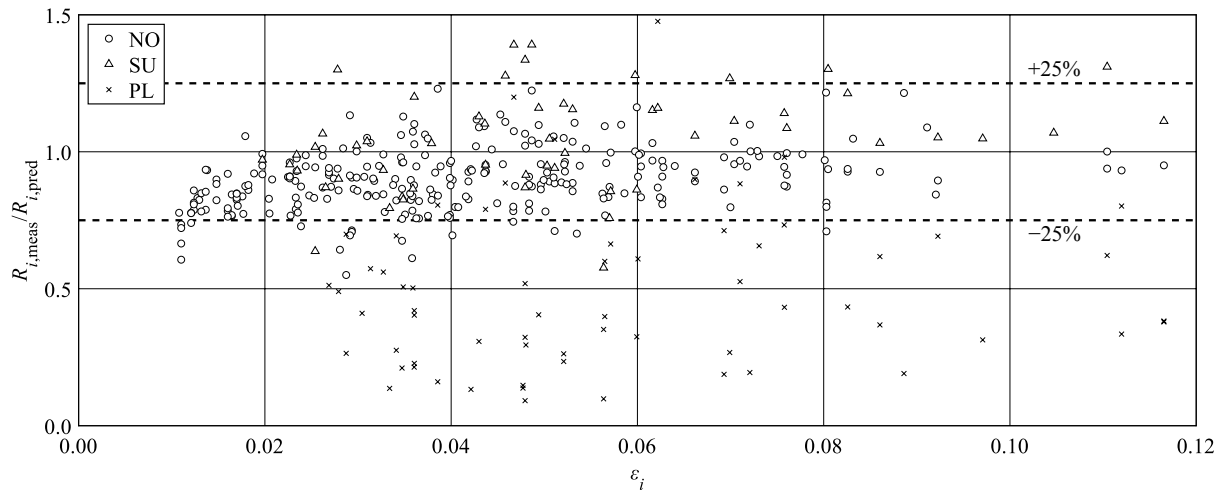


Fig. 16. Measured over predicted [Eq. (9)] run-up height $R_{i,meas}/R_{i,pred}$ versus relative wave crest amplitude ε_i for all non-breaking (NO) waves, surging breakers (SU), and plunging breakers (PL) of the present study

Discussion

Impulse Wave Trains

The application of the present study focuses on the impulse wave run-up at dam structures. As the freeboard is usually just a few meters, small waves can already be critical for dam overtopping. Therefore, target relative wave crest amplitudes were $\varepsilon_i < 0.1$ (Table 2). Although the generated wave trains consist of several wave crests and troughs, the single waves clearly differ from each other with respect to their individual wave crest celerities (Fig. 7). Compared to the leading wave crest celerity, the second, third, and fourth waves were on average 24%, 37%, and 47% slower, respectively. This decreasing trend from the front to the back of the wave train was also observed in previous studies. Fritz *et al.* (2004) conducted 2D wave channel experiments and found that the leading wave crest celerity is on average larger than the shallow-water wave celerity ($0.8 < c_1/(gh)^{1/2} < 1.5$) and can be approximated by the solitary wave celerity. The second wave crest celerity was about 20%–30% lower ($0.6 < c_2/(gh)^{1/2} < 1$). Based on 3D wave basin experiments, Mohammed and Fritz (2012) observed $0.8 < c_1/(gh)^{1/2} < 1.2$, $0.65 < c_2/(gh)^{1/2} < 0.97$, and $0.5 < c_3/(gh)^{1/2} < 0.93$ for the first, second, and third wave, respectively. The celerity of the second wave crest was on average 18%–23% lower than the leading wave crest celerity, while the third wave was about 22%–35% slower than the leading one. The reduction of the wave celerity was explained due to the decreasing wavelengths from the front to the back of the wave train, resulting in frequency dispersion. McFall and Fritz (2016) came to similar results, with the second wave being on average 23% slower than the first wave. Evers *et al.* (2019a) compared the measured first and second wave crest celerity with the solitary wave celerity c_{sol} and found that on average $c_1 = 0.95c_{sol}$ and $c_2 = 0.7c_{sol}$, respectively. This matches well with the present findings, for which the wave crest celerity of wave i within the wave train may be predicted by

$$\frac{c_i}{\sqrt{gh}} = \tilde{C}_i \sqrt{1 + \varepsilon_i}, \quad (10)$$

where \tilde{C}_i follows from Fig. 7 for the first four waves, i.e. $\tilde{C}_1 = 0.97$, $\tilde{C}_2 = 0.73$, $\tilde{C}_3 = 0.60$, and $\tilde{C}_4 = 0.50$. For the fifth wave, the prefactor slightly increases again with $\tilde{C}_5 = 0.57$; however, only $n_5 = 5$ data points were available. Fig. 17 shows the measured over predicted wave crest celerity $c_{i,meas}/c_{i,pred}$ versus ε_i for the present study and the data by Müller (1995). The wave crest celerity of the first waves is predicted within a scatter range of $\pm 10\%$, also for larger values of $\varepsilon_i > 0.1$ from the experiments of Müller (1995). For the subsequent waves, the scatter increases up to $\pm 25\%$.

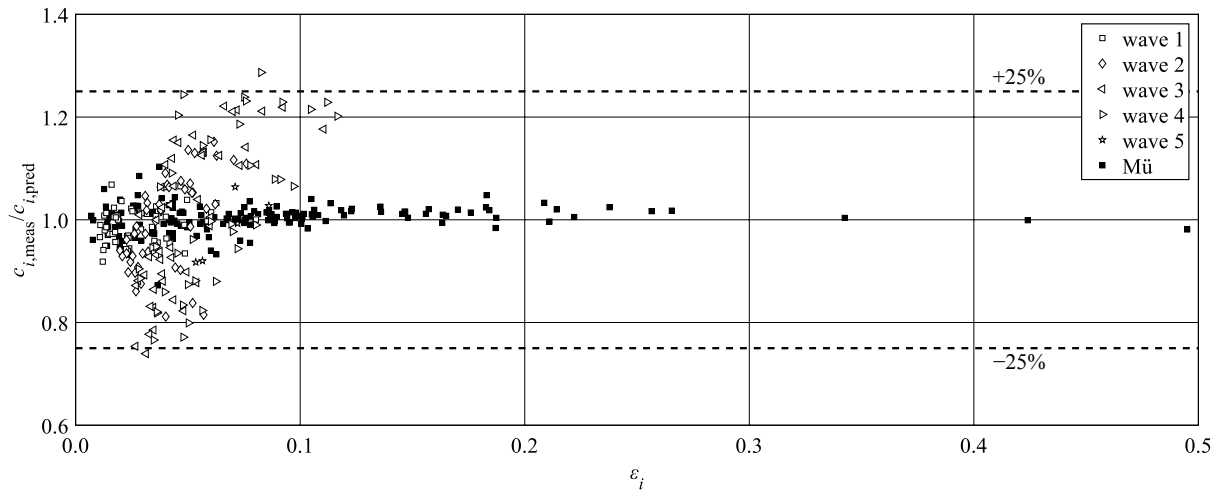


Fig. 17. Measured over predicted [Eq. (10)] wave crest celerity $c_{i,meas}/c_{i,pred}$ versus relative wave crest amplitude ε_i for the first five waves of the present study and the experiments of Müller (Mü) (1995)

The wavelengths also decrease from the front to the back of the wave train (Fig. 6) and a transition from linear intermediate-water waves to linear deep-water and Stokes-like waves was observed (Fig. 8). Heller and Hager (2011) proposed wave type classification criteria based on the wave generation parameters and distinguished between Stokes-like waves, cnoidal- or solitary-like waves, and bore-like waves. According to this approach, all impulse wave trains of the present study would be classified as Stokes-like waves, due to the small slide Froude numbers F and large still water depths h (Table 1). Considering the maximum wave crest amplitude within the $n = 49$ wave trains, the first, second, third, and fourth wave was decisive in approximately 6%, 11%, 14%, and 69% of the experiments, respectively. This is in line with previous findings, that the leading wave crest is not necessarily the maximum one for Stokes-like waves (Heller and Hager 2011). As Müller (1995) conducted similar experiments, only considering the first wave, the data is also included in Figs. 6 and 8. It is important to note that a_{c1}/H_1 of these experiments was between 0.57 and 1.00, compared to values below 0.51 for the present study (Table 2), and also larger waves with respect to L_1/h and H_1/h were generated by Müller (1995). A comparison leads to the conclusion that the leading wave propagates with about the solitary wave celerity $c_{Sol} = [gh(1 + \varepsilon)]^{1/2}$ (Fig. 7), which approaches the shallow-water wave celerity $c = (gh)^{1/2}$ for small values of ε , as in the present study (Fig. 6). With respect to wave type classification, most of the waves generated by Müller (1995) can be also classified as linear intermediate-water waves. However, larger waves lie in the areas of linear shallow-water wave, cnoidal wave, or solitary wave theory (Fig. 8). A general statement about the wave type of the leading wave can therefore not be made.

As the experiments were conducted in a wave channel, the test setup and all physical processes were considered as 2D. The energy transfer and wave propagation were unidirectional and the run-up direction was orthogonal to the barrier. In reality, this simplification might only be correct for a deep and narrow reservoir with the slide impacting on the opposite side of the dam. For general water bodies like reservoirs, both wave generation and propagation are three-dimensional (3D). The slide impact energy is transferred to a wider water column and the slide width b has a major effect on the wave generation (Evers *et al.* 2019a). The subsequent wave propagation is omnidirectional and besides the propagation distance, the wave characteristics also depend on the wave propagation angle (Huber and Hager 1997). The energy within the wave train is spread over an increasing perimeter, resulting in stronger radial wave decay (Mohammed and Fritz 2012). Heller and Spinneken (2015) found that 3D waves are considerably smaller than 2D waves for the same wave generation parameters and presented a method to transform data from 2D to 3D studies. Furthermore, for the 3D experiments only Stokes-like and cnoidal-like wave trains were observed, while solitary-like and bore-like waves additionally occurred for 2D tests with identical slide parameters. These findings emphasize the significance of Stokes-like impulse wave trains in reservoirs. Mohammed and Fritz (2012) found that the first three waves are the highest in the near field. However, as dispersion causes the location of the maximum wave crest amplitude to move backwards within the wave train with increasing propagation distance, also the fourth and following waves may be the decisive ones. An experimental observation is difficult, as the size of 2D and 3D physical models is limited and reflection of the leading wave disturbs the wave train signal at some point. The run-up of spatial impulse waves propagating radially from the impact location may be approximated with run-up equations derived from 2D experiments, if the crests of the wave train are parallel to the shore, i.e. the run-up direction is straight-on. Nevertheless, oblique wave run-up can occur, if the wave crests approach the shore at an angle in plan view. Lateral wave run-up may also be caused by edge waves directly originating from the slide impact location (Müller 1995, Lynett and Liu 2005, Heller and Spinneken 2015, McFall and Fritz 2017).

Breaker Type Prediction

Existing prediction criteria for the wave breaker type of periodic and non-periodic waves propose constant thresholds of the surf similarity parameter ξ_i (Battjes 1974; Schüttrumpf 2001; Hammeken Arana 2017). This parameter does not consider the still water depth h , which was shown to be important for the run-up of surging and non-breaking waves (Ahrens *et al.* 1993). Furthermore, the back-wash of previous waves is not included, which may be significant for mildly sloped shores and waves with short separation times. To determine ξ_i with Eq. (2), the slope angle β , the wave height H_i , and the wavelength L_i have to be known. While the former follows from the shore geometry, the latter two can be estimated with prediction equations for impulse wave generation and propagation. Fritz (2002) conducted 2D experiments with a slide impact angle $\alpha = 45^\circ$ and proposed prediction equations for the first and second wavelengths L_1 and L_2 , respectively. Furthermore, equations for a_{c2} , a_{c2}/a_{c1} , and a_{i1}/a_{ci} are given. Consequently, a prediction of the first two wave heights H_1 and H_2 is possible. Heller and Hager

(2010) provide prediction equations for the maximum wave crest amplitude and wave height of a wave train, without differentiation of the position within the wave train. For 3D wave propagation, Mohammed and Fritz (2012) proposed equations for the prediction of the first wave crest and trough amplitude a_{c1} and a_{t1} , respectively, the second wave crest amplitude a_{c2} , and the first two wavelengths L_1 and L_2 . McFall and Fritz (2016) expanded these equations for applicability to convex conical hill slopes. Evers *et al.* (2019a) presented prediction equations for a_{c1} , a_{t1} , a_{c2} , and T_1 . From the latter, the first wavelength can be determined with $L_1 = T_1 c_1$.

Applying the existing numerical values for ξ_i to distinguish between the different breaker types of the present study did not lead to satisfying results. For the new proposed breaker type prediction criterion, the thresholds of ξ_i are no longer constant, but are a function of a_{ci}/H_i and L_i/h . Consequently, also the still water depth h and the wave crest amplitude a_{ci} are included. While the former is usually known accurately, the latter can again be estimated by empirical equations, as discussed above. The side-channel recordings implied that the back-wash of previous waves had an effect on plunging breakers. However, no clear correlation between the breaker type and the wave period or the separation time between the wave crests was found.

Eqs. (6)–(8) separate between non-breaking waves, surging breakers, and plunging breakers. As wave breaking is a gradual process, these boundaries are not distinct. The proposed criteria also predicts the data by Müller (1995) correctly, where only non-breaking waves occurred (Fig. 14). It can be noted that the probability of wave breaking increases with increasing non-linearity a_{ci}/H_i and wave steepness H_i/L_i , and decreasing relative wavelength L_i/h and slope angle β . In other words, a transition from a non-breaking wave to a surging or plunging breaker is possible. The latter was only observed for $\beta < 45^\circ$ (Fig. 13). As the run-up on steep to vertical slopes was investigated, no spilling breakers were observed, which tend to occur on shores of very mild slope (Komar 1998; Hafsteinsson *et al.* 2017).

Run-up Height Prediction

The new run-up prediction equation Eq. (9) for the run-up height R_i of a wave i within the wave train is based on Eq. (1) by Evers and Boes (2019). The latter was derived based on several studies on solitary wave run-up and the experiments by Müller (1995) considering exclusively the run-up of an impulse wave train's first wave. It can be noted that for solitary waves of small amplitude, with $a_c/H = 1$ and $c_{Sol} \approx (gh)^{1/2}$, Eq. (9) reduces to Eq. (1). Considering the new approach expressed by Eq. (9), R_i/h increases with increasing relative wave crest amplitude ε_i , which is obvious. It also increases with decreasing β , as shoaling effects are stronger for milder slopes. Consequently, the wave height increases up to the shore point, finally resulting in a larger run-up. However, this only applies if the wave does not break in advance. Fig. 15 confirms this reasoning, as for each wave i the mean run-up height over the wave crest $R_{i,m}/a_{ci}$ increases with decreasing β , except for plunging breakers. It also follows that the effect of β on R_i is stronger for lower slope angles. Furthermore, decreasing non-linearity a_{ci}/H_i and relative wave crest celerity $c_i/(gh)^{1/2}$ lead to a larger relative run-up height. Although the second finding appears to be counterintuitive, no better correlation based on other parameters was found.

From Fig. 16 it follows that Eq. (9) results in a satisfying prediction of the run-up height for all non-breaking waves of the present study, with a maximum underestimation of 23% and maximum overestimation of 45%. Although the latter may seem large, it lies on the side of caution and 94% of the non-breaking data still lies within a $\pm 25\%$ scatter range. For surging breakers, an increased uncertainty in predicting the run-up height has to be considered. The maximum underestimation is 39%, while the maximum overestimation is 42%. Eighty per cent of the surging breakers are predicted with $\pm 25\%$ accuracy. The prediction quality of Eq. (9) for plunging breakers decreases significantly. It lies between -91% and $+48\%$ and only 14% of the present data lies within a scatter range of $\pm 25\%$. The experiment with the underestimated outlier was repeated. From the side-channel recording it was found that the breaking behavior is not a clear plunging breaker, but may be also classified as collapsing breaker. In general, a reasonable prediction of the run-up height of plunging breakers is not given with Eq. (9), but it serves as an upper limit considering a safety allowance. From Fig. 13 it follows that plunging breakers only occurred for slope angles $\beta = 26.6^\circ$ and 18.4° . Consequently, this breaker type is not expected for steeper dams ($\beta \geq 45^\circ$) such as concrete dams.

Besides the wave parameters a_{ci} and a_{ti} , or H_i , Eq. (9) requires the celerity of each wave for run-up prediction. With Eq. (10) and the prefactors \tilde{C}_i , the wave crest celerity can be predicted in a first step, followed by a run-up prediction using Eq. (9). Fig. 18 shows the measured over predicted run-up height $R_{i,meas}/R_{i,pred}$ versus the relative

wave crest amplitude ε_i , if Eqs. (9) and (10) are applied to all waves of the present study and the experiments from Müller (1995). As the prediction of the wave crest celerity itself underlies uncertainties (Fig. 17), the prediction quality of the run-up height is expected to decrease. However, for the non-breaking waves 94% of the run-up predictions still lie within a $\pm 25\%$ scatter range, with a maximum underestimation of 27% and a maximum overestimation of 40%. On the basis of the data by Müller (1995), it can be verified that Eqs. (9) and (10) also result in reasonable predictions of the run-up height for non-breaking waves with larger values $0.1 < \varepsilon_i < 0.5$. For surging breakers the prediction quality shifts towards underestimation and lies between -30% and $+56\%$. Eighty-four per cent of the run-up heights are predicted with $\pm 25\%$ accuracy. With respect to plunging breakers, only 8% of the run-up heights are predicted within a scatter range of $\pm 25\%$. The majority of the data is again largely overestimated, while an additional underestimated outlier can be noted.

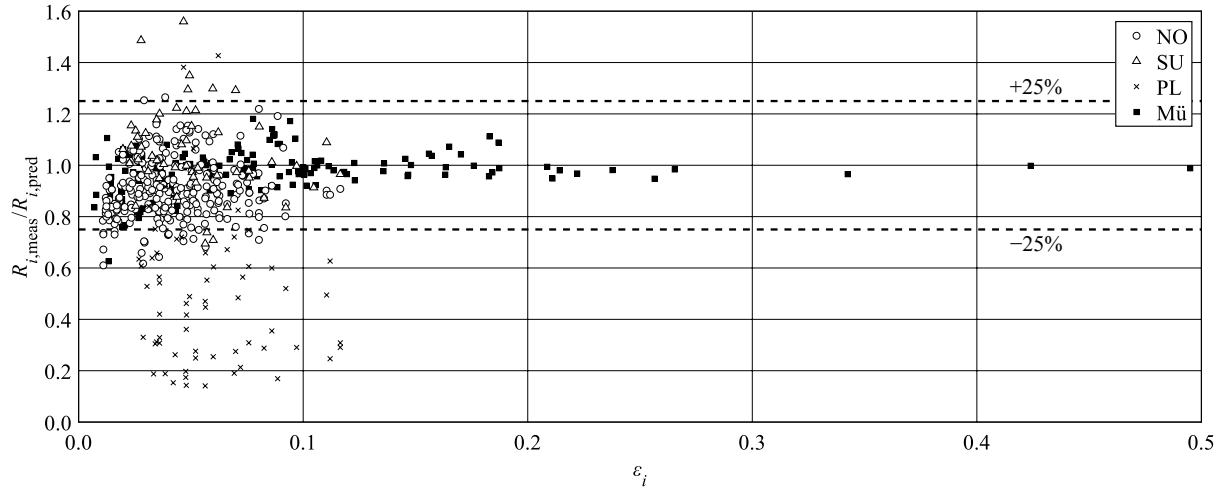


Fig. 18. Measured over predicted [Eq. (9)] run-up height $R_{i,meas}/R_{i,pred}$ versus relative wave crest amplitude ε_i , predicting the relative wave crest celerity $c_i/(gh)$ with Eq. (10), for all non-breaking (NO) waves, surging breakers (SU), and plunging breakers (PL) of the present study and the experiments of Müller (Mü) (1995)

As a comparison, Fig. 19 shows the run-up prediction applying Eq. (1) by Evers and Boes (2019) with ε as the single governing wave characteristic. As expected, R_1 is well predicted by Eq. (1) with only single experiments exceeding the prediction by up to 50% for small $\varepsilon < 0.02$. However, the measured run-up heights of the subsequent waves largely exceed the predictions. This comparison shows the necessity of taking into account the additional parameters a_{ci}/H_i and $c_i/(gh)^{1/2}$ for the run-up prediction of impulse wave trains featuring Stokes-like waves.

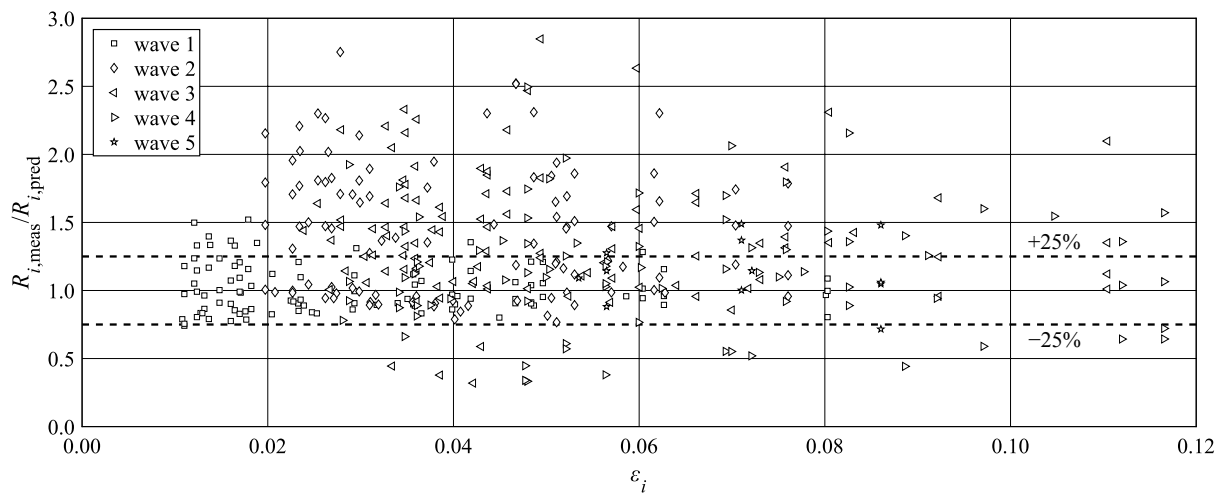


Fig. 19. Measured over predicted [Eq. (1) by Evers and Boes (2019)] run-up height $R_{i,meas}/R_{i,pred}$ versus relative wave crest amplitude ε_i for the 1st, 2nd, 3rd, 4th, and 5th wave of the present study

From the discussion above it may be concluded that non-breaking and surging-breaker waves are the relevant ones during the run-up process of an impulse wave train. With respect to the run-up height, it was shown that indeed these two types are the decisive ones. However, besides providing a sufficient freeboard, the dam or shoreline structure also has to withstand the dynamic forces caused by wave run-up. Although pressures or forces on the barrier during wave run-up were not investigated within this study, it can be assumed that plunging breakers cause the largest local loading to the structure due to the impinging water jet. The herein proposed run-up prediction equation is based on 2D run-up experiments with a plane, smooth, and impermeable slope. At prototype scale, the run-up behavior is additionally influenced by three-dimensional slope features, non-constant slopes, as well as rough and permeable run-up surfaces. Roughness effects were found negligible for solitary wave run-up on relatively steep slopes ($\beta \geq 20^\circ$), while they may be significant for milder slope angles (Teng *et al.* 2000). Strong curvatures along the shoreline cause flow diversion and concentration, which might lead to a significant over- or underestimation of the actual run-up height (Evers and Boes 2019). Therefore, the present findings and developed equations should only be applied to evenly formed shore conditions. For the run-up height prediction with Eqs. (9) and (10), a safety margin of +25% for non-breaking waves and +50% for surging and plunging breakers needs to be considered. Uncertainties due to the estimation of the governing wave parameters have to be considered additionally.

Conclusions

Within this study, the run-up behavior of impulse wave trains on a plane and impermeable barrier with slope angles β between 18.4° and 90° was investigated. First, $n = 49$ unconfined wave trains were generated. As the application of the present study focuses on impulse waves in reservoirs with a freeboard of only a few meters at the dam, small waves can already be critical for dam overtopping. Therefore, target relative wave crest amplitudes were $\varepsilon_i < 0.1$. In a second step, $n = 101$ run-up experiments were conducted with the same wave generation parameters, but various barrier slopes. As different run-up behavior was observed, breaker type prediction criteria were proposed for non-breaking waves, surging breakers, and plunging breakers. Furthermore, a prediction equation for the run-up of the first five waves within a wave train was presented. The new equations were validated for the first wave crest with the experiments by Müller (1995). Provided that the individual wave parameters can be estimated, a prediction of the maximum run-up height due to an imminent impulse wave event is possible. Accordingly, a sufficient freeboard can be dimensioned or an adequate preemptive reservoir drawdown can be initiated. The main findings of the present study are:

- Small impulse wave trains can be usually classified as Stokes-like waves, for which the leading wave is not necessarily the one of maximum crest amplitude.
- The number of breaking waves increases with decreasing β , with a transition from non-breaking waves to surging and plunging breakers.
- Non-breaking waves and surging breakers cause the largest run-up heights.
- The proposed run-up equation predicts the run-up height of non-breaking waves and surging breakers with a maximum underestimation of 25% and 40%, respectively. For plunging breakers, which only occurred for $\beta < 45^\circ$, it may serve as an upper limit.

Data Availability Statement

Some or all data, models, or code generated or used during the study are available in a repository or online in accordance with funder data retention policies (Kastinger *et al.* 2020, DOI: 10.5281/zenodo.3444029).

Acknowledgments

This work was supported by the Swiss Federal Office of Energy SFOE / Bundesamt für Energie BFE within its Hydropower research programme (Project No. SI/501945-01) and is part of the Swiss Competence Center for Energy Research – Supply of Electricity (SCCER-SoE). The first author was supported by the Excellence Scholarship & Opportunity Programme (ESOP) at ETH Zurich for a pilot study.

Notation

The following symbols are used in this paper:

a_{ci} = wave crest amplitude of wave i (m);

a_{ti} = wave trough amplitude of wave i (m);

b = slide width (m);

c_i = wave crest celerity of wave i (m/s);

$c_{i,\text{meas}}$ = measured wave crest celerity of wave i (m/s);

$c_{i,\text{pred}}$ = predicted wave crest celerity of wave i (m/s);

c_R = run-up celerity (m/s);

c_{Sol} = solitary wave celerity, $c_{\text{Sol}} = [g(h + a_c)]^{1/2}$ (m/s);

C_i = wave crest celerity of wave i over solitary wave celerity, $C_i = c_i / [g(h + a_{ci})]^{1/2}$;

\tilde{C}_i = median value of C_i ;

F = slide Froude number, $F = V_s/(gh)^{1/2}$;

F_{max} = maximum slide Froude number;

g = gravitational acceleration (m/s²);

h = still water depth (m);

h_{min} = minimum still water depth (m);

h_R = run-up tongue thickness (m);

H_i = wave height of wave i (m);

H_{min} = minimum wave height (m);

i = wave position within the wave train ($i = 1$ to 5);

L_i = wavelength of wave i (m);

L_{min} = minimum wavelength (m);

m_s = slide mass (kg);

M = relative slide mass, $M = m_s/(\rho_w b h^2)$;

n = number of experiments, porosity (%);

n_i = number of experiments for wave i ;

P = impulse product parameter (Heller and Hager 2010), $P = FS^{1/2}M^{1/4}\{\cos[(6/7)\alpha]\}^{1/2}$;

R_i = run-up height of wave i (m);

$R_{i,m}$ = mean run-up height of wave i (m);

$R_{i,\text{max}}$ = maximum run-up height of wave i (m);

$R_{i,\text{meas}}$ = measured run-up height of wave i (m);

$R_{i,\text{min}}$ = minimum run-up height of wave i (m);

$R_{i,\text{pred}}$ = predicted run-up height of wave i (m);

R^2 = coefficient of determination;

R_R = run-up Reynolds number, $R_R = c_R h_R / \nu$;

$R_{R,\text{min}}$ = minimum run-up Reynolds number;

s = slide thickness (m);

S = relative slide thickness, $S = s/h$;

t = time (s);

t_r = residence time (s);

T_i = wave period of wave i (s);

T_{min} = minimum wave period (s);

V_s = slide impact velocity (m/s);

$V_{s,\text{max}}$ = maximum slide impact velocity (m/s);

W_R = run-up Weber number, $W_R = \rho_w c_R^2 h_R / \sigma$;

$W_{R,\text{min}}$ = minimum run-up Weber number;

x = streamwise coordinate (m);

z = vertical coordinate (m);

α = slide impact angle ($^\circ$);

β = shore slope angle ($^\circ$);

Δz = drop height (m);

ε_i = relative wave crest amplitude of wave i , $\varepsilon_i = a_{ci}/h$;

η = water surface displacement (m);

ν = kinematic water viscosity (m^2/s);

ρ_g = grain density (kg/m^3);

ρ_s = bulk slide density (kg/m^3);

ρ_w = water density (kg/m^3);

σ = water surface tension (kg/s^2); and

ζ_i = surf similarity parameter of wave i (Iribarren and Nogales 1949), $\zeta_i = \tan\beta/(H_i/L_i)^{1/2}$.

References

- Achterberg, D., Gotzmer, J. W., Spath, R., Tseng, M., Woodward, D. E., Miller, N., and Shipman, S. A. (1998). "Federal guidelines for dam safety: selecting and accommodating inflow design floods for dams." Dept. of Homeland Security, Federal Emergency Management Agency, Washington, DC.
- Ahrens, J. P., Seelig, W. N., Ward, D. L., and Allsop, N. W. H. (1993). "Wave runup on and wave reflection from coastal structures." *Proc., Ocean Wave Measurement and Analysis*, American Society of Civil Engineers, 489–502.
- Battjes, J. A. (1974). "Surf similarity." *Proc., 14th Int. Conf. Coastal Engineering*, 1, 466–480. Reston, VA: ASCE.
- Bregoli, F., Bateman, A., Medina, V. (2017). "Tsunamis generated by fast granular landslides: 3D experiments and empirical predictors." *J. Hydraul. Res.*, 55, 743–758. <https://doi.org/10.1080/00221686.2017.1289259>.
- Chen, Y. Y., Kharif, C., Yang, J. H., Hsu, H. C., Touboul, J., and Chambarel, J. (2015). "An experimental study of steep solitary wave reflection at a vertical wall." *European Journal of Mechanics - B/Fluids*, 49, 20–28. <https://doi.org/10.1016/j.euromechflu.2014.07.003>.
- Coppola, L., Filardi, A., Bromhead, E. N. (2013). "Landslide and Flood Hazard from the Lago Sirino, Basilicata, Italy." *Italian Journal of Engineering Geology and Environment*, 6, 393–398. <https://doi.org/10.4408/IJEGE.2013-06.B-37>.
- Davidson, D. D., and McCartney, B. L. (1975). "Water waves generated by landslides in reservoirs." *Journal of the Hydraulics Division, ASCE*, 101(WW12), 1489–1501.
- Evers, F. M., and Boes, R. M. (2019). "Impulse Wave Runup on Steep to Vertical Slopes." *Journal of Marine Science and Engineering*, 7, 8. <https://doi.org/10.3390/jmse7010008>.
- Evers, F. M., and Hager, W. H. (2015). "Impulse wave generation: Comparison of free granular with mesh-packed slides." *J. Mar. Sci. Eng.*, 3, 100–110. <https://doi.org/10.3390/jmse3010100>.
- Evers, F. M., Hager, W. H., and Boes, R. M. (2019a). "Spatial Impulse Wave Generation and Propagation." *J. Waterway, Port, Coastal, Ocean Eng.*, 145(3), 04019011. [https://doi.org/10.1061/\(ASCE\)WW.1943-5460.0000514](https://doi.org/10.1061/(ASCE)WW.1943-5460.0000514).
- Evers, F. M., Heller, V., Fuchs, H., Hager W. H., and Boes, R. M. (2019b). "Landslide-generated impulse waves in reservoirs - Basics and computation." *VAW-Mitteilung 254* (R. Boes, ed.), ETH Zurich, Zürich. <https://doi.org/10.3929/ETHZ-B-000413216>.
- Evers, F. M., Schmocker, L., Fuchs, H., Schwegler, B., Fankhauser, A. U., and Boes, R. M. (2018). "Landslide generated impulse waves: assessment and mitigation of hydraulic hazards." *Proc., ICOLD Congress*, Paris: ICOLD International Commission on Large Dams. <https://doi.org/10.3929/ETHZ-B-000276308>.
- Fritz, H. M. (2002). "Initial phase of landslide generated impulse waves." *VAW-Mitteilung 178* (H.-E. Minor, ed.), ETH Zurich, Zürich.
- Fritz, H. M., and Borrero, J. C. (2006). "Somalia field survey after the December 2004 Indian Ocean tsunami." *Earthquake Spectra*, 22(S3), 219–233. <https://doi.org/10.1193/1.2201972>.
- Fritz, H. M., Giachetti, T., Anderson, S. A., and Gauthier, D. (2018). "Field survey of the 17 June 2017 landslide generated Tsunami in Karrat Fjord, Greenland." In *EGU General Assembly Conference Abstracts*, 20, 18345. Munich, Germany: EGU European Geosciences Union.

- Fritz, H. M., Hager, W. H., and Minor, H. E. (2004). "Near field characteristics of landslide generated impulse waves." *J. Waterway, Port, Coastal, Ocean Eng.*, 130(6), 287-302. [https://doi.org/10.1061/\(ASCE\)0733-950X\(2004\)130:6\(287\)](https://doi.org/10.1061/(ASCE)0733-950X(2004)130:6(287)).
- Fuchs, H., Boes, R. M., and Pfister, M. (2011). "Impulse waves at Kühtai reservoir generated by avalanches and landslides." *Proc., International Symposium on Dams and Reservoirs under Changing Challenges*, CRC Press, Taylor & Francis Group, 701–708.
- Fuchs, H., and Hager, W. H. (2015). "Solitary impulse wave transformation to overland flow." *J. Waterway, Port, Coastal, Ocean Eng.*, 141(5), 04015004. [https://doi.org/10.1061/\(ASCE\)WW.1943-5460.0000294](https://doi.org/10.1061/(ASCE)WW.1943-5460.0000294).
- Galvin, J. C. (1968). "Breaker type classification on three laboratory beaches." *Journal of Geophysical Research*, 73(12), 3651–3659. <https://doi.org/10.1029/JB073i012p03651>.
- Hafsteinsson, H. J., Evers, F. M., and Hager, W. H. (2017). "Solitary wave run-up: wave breaking and bore propagation." *Journal of Hydraulic Research*, 55(6), 787–798. <https://doi.org/10.1080/00221686.2017.1356756>.
- Hall, J.V., and Watts, G.M. (1953). "Laboratory Investigation of the Vertical Rise of Solitary Wave on Impermeable Slopes." *Technical Memo Report No. 33*; U.S. Army Corps of Engineers, Beach Erosion Board: Washington, DC.
- Hammeken Arana, A. M. (2017). "Wave run-up on beaches and costal structures." *PhD Thesis*, Dept. of Civil, Environmental and Geomatic Engineering, University College London.
- Heller, V. (2008). "Landslide generated impulse waves: Prediction of near field characteristics." *VAW-Mitteilung* 204, edited by H.-E. Minor. Zürich, Switzerland: ETH Zurich.
- Heller, V., and Hager, W. H. (2010). "Impulse product parameter in landslide generated impulse waves." *J. Waterway, Port, Coastal, Ocean Eng.*, 136(3), 145–155. [https://doi.org/10.1061/\(ASCE\)WW.1943-5460.0000037](https://doi.org/10.1061/(ASCE)WW.1943-5460.0000037).
- Heller, V., and Hager, W. H. (2011). "Wave types of landslide generated impulse waves." *Ocean Engineering*, 38(4): 630–640. <https://doi.org/10.1016/j.oceaneng.2010.12.010>.
- Heller, V., Hager W. H., and Minor, H.-E. (2009). "Landslide generated impulse waves in reservoirs: Basics and computation." *VAW-Mitteilung* 211 (H.-E. Minor, ed.), ETH Zurich, Zürich.
- Heller, V., and Spinneken, J. (2015). "On the effect of the water body geometry on landslide–tsunamis: Physical insight from laboratory tests and 2D to 3D wave parameter transformation." *Coastal Engineering*, 104, 113–134. <https://doi.org/10.1016/j.coastaleng.2015.06.006>.
- Higman, B., Shugar, D. H., Stark, C. P., Ekström, G., Koppes, M. N., Lynett, P., Dufresne, A., Haeussler, P. J., Geertsema, M., Gulick, S., Mattox, A., Venditti, J. G., Walton, M. A. L., McCall, N., Mckittrick, E., MacInnes, B., Bilderback, E. L., Tang, H., Willis, M. J., Richmond, B., Reece, R. S., Larsen, C., Olson, B., Capra, J., Aycia, A., Bloom, C., Williams, H., Bonno, D., Weiss, R., Keen, A., Skanavis, V., and Loso, M. (2018). "The 2015 landslide and tsunami in Taan Fiord, Alaska." *Sci. Rep. UK*, 8, 12993. <https://doi.org/10.1038/s41598-018-30475-w>.
- Huber, A., and Hager, W. H. (1997). "Forecasting impulse waves in reservoirs." *Proc., 19th Congrès des Grands Barrages*, C.31: 993-1006. Paris: ICOLD International Commission on Large Dams.
- Hunt, I. A. (1959). "Design of seawalls and breakwaters." *Journal of the Waterways and Harbors Division*, 85(3), 123–152.
- Iribarren, C. R., and Nogales, C. (1949). "Protection des ports (Harbour protection)." *Proc. 17th Int. Navigation Congress*, 31–80. Bruxelles, Belgium: PIANC Permanent International Association of Navigation Congresses. (In French).

- Kasting, M. B. A., Evers, F. M., Boes R. M. (2020). "Hydraulic scale model experiments on the two-dimensional run-up of impulse wave trains on steep to vertical slopes [dataset]." *Zenodo*. <https://doi.org/10.5281/zenodo.3444029>.
- Kobel, J., Evers, F. M., and Hager, W. H. (2017). "Impulse Wave Overtopping at Rigid Dam Structures." *J. Hydraulic Eng.*, 143(6). 04017002. [https://doi.org/10.1061/\(ASCE\)HY.1943-7900.0001271](https://doi.org/10.1061/(ASCE)HY.1943-7900.0001271).
- Komar, P. D. (1998). *Beach processes and sedimentation*, Prentice Hall, New Jersey.
- Le Méhauté, B. (1976). *An Introduction to Hydrodynamics and Water Waves*, Springer Science+Business Media, New York. <https://doi.org/10.1007/978-3-642-85567-2>.
- Lo, H.-Y., Park, Y. S., Liu, P. L.-F. (2013). "On the run-up and back-wash processes of single and double solitary waves – An experimental study." *Coastal Engineering*, 80, 1-14. <https://doi.org/10.1016/j.coastaleng.2013.05.001>.
- Lockridge, P. A. (1990). "Nonseismic Phenomena in the Generation and Augmentation of Tsunamis." *Natural Hazards*, 3(4), 403–412. <https://doi.org/10.1007/BF00124396>.
- Løvholt, F., Pedersen, G., and Gisler, G. (2008). "Oceanic propagation of a potential tsunami from the La Palma Island." *J. Geophys. Res.*, 113, C09026. <https://doi.org/10.1029/2007JC004603>.
- Lynett, P., and Liu, P. L. F. (2005). "A numerical study of the run-up generated by three-dimensional landslides." *Journal of Geophysical Research: Oceans*, 110, C03006. <https://doi.org/10.1029/2004JC002443>.
- McCowan, J. (1894). "On the highest wave of permanent type." *The London, Edinburgh, and Dublin Philosophical Magazine and Journal of Science*, 38:233, 351-358. <https://doi.org/10.1080/14786449408620643>.
- McFall, B. C., and Fritz, H. M. (2016). "Physical modelling of tsunamis generated by three-dimensional deformable granular slides on planar and conical island slopes." *Proc. R. Soc. A*, 472, 20160052. <https://doi.org/10.1098/rspa.2016.0052>.
- McFall, B. C., and Fritz, H. M. (2017). "Runup of granular landslide-generated tsunamis on planar coasts and conical islands." *J. Geophys. Res. Oceans*, 122(8), 6901-6922. <https://doi.org/10.1002/2017JC012832>.
- Miller, D. J. (1960). "The Alaska earthquake of July 10, 1958: giant wave in Lituya Bay." *Bulletin of the Seismological Society of America*, 50(2), 253–266.
- Mohammed, F., and Fritz, H. M. (2012). "Physical modeling of tsunamis generated by threedimensional deformable granular landslides." *Journal of Geophysical Research: Oceans*, 117(C11), 1–20. <https://doi.org/10.1029/2011jc007850>.
- Müller, D. R. (1995). "Auflaufen und Überschwappen von Impulswellen an Talsperren (Run-up and overtopping of impulse waves at dams)." *VAW-Mitteilung* 137 (D. Vischer, ed.), ETH Zurich, Zürich (in German).
- Neelamani, S. (2005). "Subareal wave pressures, layer thicknesses, run-up and run-down velocity on sea walls." *Indian Journal of Marine Sciences*, 34(3), 299–309.
- Panizzo, A., De Girolamo, P., Di Risio, M., Maistri, A., Petaccia, A. (2005). "Great landslide events in Italian artificial reservoirs." *Natural Hazards and Earth System Science*, 5, 733–740. <https://doi.org/10.5194/nhess-5-733-2005>.
- Pougatsch, H., Ammann, E., Hauenstein, W., Loosli, D., Mouvet, L., Müller, R. W., and Rechsteiner, G. (2002). "Sicherheit der Stauanlagen. Basisdokument zur konstruktiven Sicherheit [Dam safety. Base document on structural safety]." Federal Office for Water and Geology, Biel, Switzerland (in German).

Pujara, N., Liu, P. L.-F., and Yeh, H. (2015). "The swash of solitary waves on a plane beach: Flow evolution, bed shear stress and run-up." *J. Fluid Mech.*, 779, 556–597. <https://doi.org/10.1017/jfm.2015.435>.

Roberts, N. J., McKillop, R., Hermanns, R. L., Clague, J. J., and Oppikofer, T. (2014). "Preliminary global catalogue of displacement waves from subaerial landslides." *Landslide Science for a Safer Geoenvironment* (K. Sassa, P. Canuti, Y. Yin, eds.), 687–692. Cham, Switzerland: Springer. https://doi.org/10.1007/978-3-319-04996-0_104.

Roberts, N. J., McKillop, R. J., Lawrence, M. S., Psutka, J. F., Clague, J. J., Brideau, M.-A., and Ward, B. C. (2013). "Impacts of the 2007 landslide-generated tsunami in Chehalis Lake, Canada." *Landslide Science and Practice* 6 (C. Margottini, P. Canuti, K. Sassa, eds.), 133–140. Berlin: Springer. https://doi.org/10.1007/978-3-642-31319-6_19.

Savitzky, A., Golay, M. J. E. (1964). "Smoothing and Differentiation of Data by Simplified Least Squares Procedures." *Analytical Chemistry*, 36(8), 1627–1639. <https://doi.org/10.1021/ac60214a047>.

Schüttrumpf, H. (2001). "Wellenüberlaufströmung bei Seedeichen – Experimentelle und theoretische Untersuchungen (Wave overtopping flow at sea dikes – Experimental and theoretical investigations)." *PhD Thesis*, Leichtweiß-Institut für Wasserbau, Technische Universität Braunschweig, Braunschweig (In German). <https://nbn-resolving.org/urn:nbn:de:gbv:084-15802>.

Stagonas, D., Warbick D., Muller, G., Magagna, D. (2011). "Surface tension effects on energy dissipation by small scale, experimental breaking waves." *Coastal Engineering*, 58, 826–836. <https://doi.org/10.1016/j.coastaleng.2011.05.009>.

Synolakis, C.E. (1987). "The runup of solitary waves." *Journal of Fluid Mechanics*, 185(Dec), 523–545. <https://doi.org/10.1017/S002211208700329X>.

Teng, M. H., Feng, K., and Liao, T. I. (2000). "Experimental Study on Long Wave Run-up on Plane Beaches." *Proc., 10th International Offshore and Polar Engineering Conference*, The International Society of Offshore and Polar Engineers, Seattle, WA, 660–664.

Volkart, P. (1975). "Überschwappvorgänge infolge Lawinen- und Eisniedergängen in alpinen Staubecken (Overtopping due to avalanches and ice slides into alpine reservoirs)." *Proc., Interpraevent '75*, 255–270. Klagenfurt, Austria: Research Association for Preventive Action against Flooding (in German).

Walters, R. C. S. (1971). *Dam geology*, Butterworth, London.

Ward, S. N. (2001). "Landslide tsunami." *J. Geophys. Res.*, 106(6), 11,201–11,215. <https://doi.org/10.1029/2000JB900450>.

Wiegel, R. L. (1964). *Oceanographical Engineering*, Prentice Hall, New Jersey.